Optothermal Characterization of Nanoparticle Infused Aerogels

MUBARIZ AHMAD NAGI

A THESIS SUBMITTED TO
THE FACULTY OF GRADUATE STUDIES
IN PARTIAL FULFILLMENT OF THE REQUIREMENTS
FOR THE DEGREE OF
MASTER OF APPLIED SCIENCE

GRADUATE PROGRAM IN MECHANICAL ENGINEERING
YORK UNIVERSITY
TORONTO, ONTARIO

August 2023

Abstract

Here, custom fabricated nanoparticle infused aerogels are presented as a potential material to achieve super insulating and transparent opto-thermal properties. By incorporating nanoparticle solutions within the silicon dioxide (SiO_2) aerogel during the sol-gel process, unique monolithic samples were fabricated and opto-thermally characterized. The pure silica and nanoparticle infused (Zinc Oxide, Antimony doped Tin Oxide, Zirconia Dioxide) silica aerogel samples, through UV-Vis and FTIR measurements, spectrophotometrically demonstrated a solar weighted transmittance of 86, 86, 55 and 78% with measured effective thermal conductivity values of 0.035, 0.050, 0.045, 0.045 W/(m·K) with an error threshold of ± 0.005 W/(m·K) using a modified guarded hot-plate technique respectively. The inclusion of nanoparticles within SiO_2 aerogels results in reduced transmission (heat loss) in the mid-infrared (MIR) while maintaining high transmission in the visible wavelength region. Importantly, the results show that nanoparticle infusion can be used as a flexible method to tailor the opto-thermal properties of aerogels.

Acknowledgements

I would like to thank my supervisors Dr. Thomas A. Cooper and Dr. Marina Freire-Gormaly and my co-supervisor Professor Paul O'Brien for giving me the opportunity to further my knowledge and education in the field of mechanical engineering. Without their unwavering guidance, expertise, and patience, this work would not have been possible. I find myself lucky to have had supervisors that genuinely were involved in my research with the knowledge and experience required for quality discussions and direction.

As a note, I would like to thank the thermal fluids lab at York University run by Dr. Kempers as well as his student Mouaz for assisting in the thermal conductivity measurements. Thank you for your help and contribution to this work.

I would also like to extend my sincere appreciation to the lab and faculty members Theresa, Matteo, Perry, Taz, Ikbal, Anna, Gianpaolo, Mehran, Amanda, Claudia, and Yvonne at York University. Their engaging discussions, support, and valuable resources encouraged me to further my depth of research.

Additionally, I want to acknowledge the assistance of my close friends David, Gianpaolo, Cindy, Sara, Raheel, Tahir and all my friends who have been by my side during the ups and downs of this academic endeavor. Your continuous encouragement and moral support have been pivotal and a constant source of motivation for the completion of this work.

A special thanks goes out to Mr. Oh, my high school physics teacher who motivated me to pursue mechanical engineering. Thank you for inspiring me to become an engineer.

I would like to acknowledge the support and understanding of my family. To my mother and father Aneela and Khalid who pushed me to pursue a masters, and my sisters Madiha and Sabiha for their consistent support. Their unwavering belief in my abilities and sacrifices made this academic pursuit a reality.

Finally, I am deeply grateful to Allah for his grace and guidance throughout the process of completing my education. His constant presence has given me the strength to overcome challenges and reach this significant milestone. Nothing I have accomplished would be possible without him.

Table of Contents

List of Tables

List of Figures

Equation Nomenclature

A	Wavelength independent Coefficient	–
A	Sample Cross Sectional Area	m^2
a	Radius of nanoparticle	nm
B	Extinction Contribution Coefficient	–
B_λ	Spectral Extinction Coefficient	mm^{-1}
c	Curve Fit Coefficient	–
d	Diameter of scattering center	nm
I_t	Transmitted Light Intensity	cd
I_0	Incident Light Intensity	cd
k_{eff}	Effective Thermal Conductivity	W/(m·K)
κ_λ	Absorption Coefficient	nm^{-1}
λ	Wavelength	nm^{-1}
L	Sample Thickness	m
n	Relative Refractive Index	–
$\sigma_{\lambda,sca}$	Spectral Scattering Coefficient	nm^{-1}
ρ_{ap}	Apparent Density	kg/m^3
ρ_{SiO_2}	Density of amorphous silica	kg/m^3
Q	Measured Input Electrical Power	W
R_c	Contact Resistance	$(m^2 \cdot K)/W$
s	Sample Thickness	mm
T	Temperature	°C
τ	Transmittance	%
τ_λ	Spectral Transmittance	%
t_o	Optical Thickness	–
x	Characteristic Size	–

Abbreviations

ASTM	American Society for Testing Materials
FTIR	Fourier Transform InfraRed Spectroscopy
IR	InfraRed
MIR	Mid InfraRed
MIT	Massachusetts Institute of Technology
NIR	Near InfraRed
NP	Nanoparticle
PPE	Personal Protective Equipment
RTD	Resistance Temperature Detector
RTE	Radiative Transport Equation
SDS	Safety Data Sheet
SEM	Scanning Electron Microscopy
UOB	University of Bath
UV	Ultra-Violet
UV-VIS	Ultra-Violet Visible Spectroscopy

Chemical Abbreviations

ATO	Antimony doped Tin-Oxide
CO_2	Carbon Dioxide
EtOH	Ethanol
H_2O	Water
HPLC	High Performance Liquid Chromatography
MeOH	Methanol
MTES	Methyl Tri Ethoxy Silane
MTMS	Methyl Tri Methoxy Silane
NH_3	Ammonia
NH_3 2 M in MeOH	Ammonia Solution *alternatively* Ammonia 2 Molar in Methanol
NH_4OH	Ammonium Hydroxide
PTFE	Poly Tetra Fluoro Ethylene
PTMS	Phenyl Tri Methoxy Silane
SiO_2	Silica Dioxide
TEOS	Tetra Ethyl Ortho Silicate
TMOS	Tetra Methyl Ortho Silicate
ZnO	Zinc Oxide
ZrO_2	Zirconia Dioxide

Chapter 1 – Introduction

In 2021, global primary energy consumption reached over 600 billion gigajoules, an increase of roughly 5.5% compared to 2020, with 30% of energy consumption being in building operation [1],[2]. As the rate of global energy usage continues to rise, the need for sustainable solutions becomes increasingly urgent. Emerging technologies and materials offer new opportunities for optimizing energy consumption, energy efficiency and reducing greenhouse gas emissions. With the demand for innovative materials, it is essential to explore new means of material selection and optimization to address the challenges of energy conservation. Heat loss, being one of the largest contributors to energy waste in sectors such as residential and commercial buildings [3], presents a significant opportunity for improvement, especially in real estate boom regions with high rise buildings focused on window-based aesthetic. To achieve energy-efficient buildings, there is a pressing need for materials that can function as high performing insulators within the infrared while maintaining transparency in visible light. Materials such as aerogels would allow for effective thermal insulation while still enabling the penetration of natural light, resulting in reduced energy consumption and improved comfort in comparison to existing soda-lime glass windows. In this context, this thesis aims to contribute to the development and understanding of silica aerogel monoliths, focusing on the synthesis and characterization of nanoparticle infused monoliths, for sustainable opto-thermal applications.

In brief, pure silica and nanoparticle infused silica aerogel monoliths are to be synthesized using supercritical drying. Where monoliths are defined as large homogenous slabs of aerogel and supercritical drying is the procedure in which liquid is super-critically evacuated from the aerogel's pores. The monoliths are then optically and thermally measured. The direct and hemispherical transmittance are measured. Where direct transmittance is the amount of normal light that passes through the monolith. Hemispherical transmittance includes direct transmittance with the addition of diffuse light that may have scattered due to the aerogel's inherent properties. The effective thermal conductivity is also measured. Where effective thermal conductivity defines how much radiative and conductive heat transport through the aerogel.

1.1 Motivation

Over the years, aerogels have undergone significant advancements aimed at addressing challenges related to manufacturing expenses, cost-effectiveness, and optimization of fabrication procedures. These unique materials possess tremendous potential to enhance multiple fields (aerospace, energy storage, environmental remediation, and biomedical applications) and contribute to the development of more energy-efficient technologies. While aerogels already offer benefits to industries such as commercial and residential buildings by enabling heat absorption in the infrared region, there remains a trade-off with visible light transmittance [4]. To overcome this limitation, the optimization of aerogels and post-processing techniques to enhance transmittance and thermal conductivity have been extensively studied [5], yet there is still room for further improvement. Considering this, the idea of incorporating nanoparticle suspensions within the aerogel matrix emerged as a potential solution to strike an ideal balance between visible light transmittance and infrared absorbance. By exploring this avenue, this research aims to contribute to the ongoing efforts in advancing aerogel technology and unlocking their full potential for enhancing energy efficiency in various opto-thermal applications.

1.2 Literature Review

This section discusses the latest advancements in aerogel synthesis techniques, providing some background on the exploration of various methods and recipes. It examines the recent developments in the field, including modifications and optimizations in the synthesis process to enhance the properties of aerogels.

In the paper provided by Buratti et al., a comprehensive review of current aerogel synthesis as well as thermal and optical properties is provided [6]. Aerogels ranging from recipes based on varying precursors such as Tetramethal Orthosilicate (TMOS), Tetraethyl Orthosilicate (TEOS) and Methyltrimethoxysilane (MTES) to defining different drying techniques and extraction methods are discussed. The key monolithic recipe to silica aerogel synthesis discussed was by TMOS base catalysis and supercritical drying. Based on their summation of production processes for aerogels, one can understand that there has been thorough research and development done on optimizing pure silica aerogels specifically for glazed window-based applications. Monolithic samples measured at near 20 mm in thickness showcased a thermal conductivity of approximately 0.016 W/(m·K) [6]. Further testing for optical properties with thinner samples

ranging in 7-12 mm in thickness were conducted and gave hemispherical solar transmittance varying from 86-92 % and direct solar transmittance values ranging from 3-19% [6]. Buratti et al. made it apparent that monolithic aerogels have room for improvement compared to glazed systems depending on how fabrication procedure is conducted specifically in optimizing thermal conductivity and scattering properties.

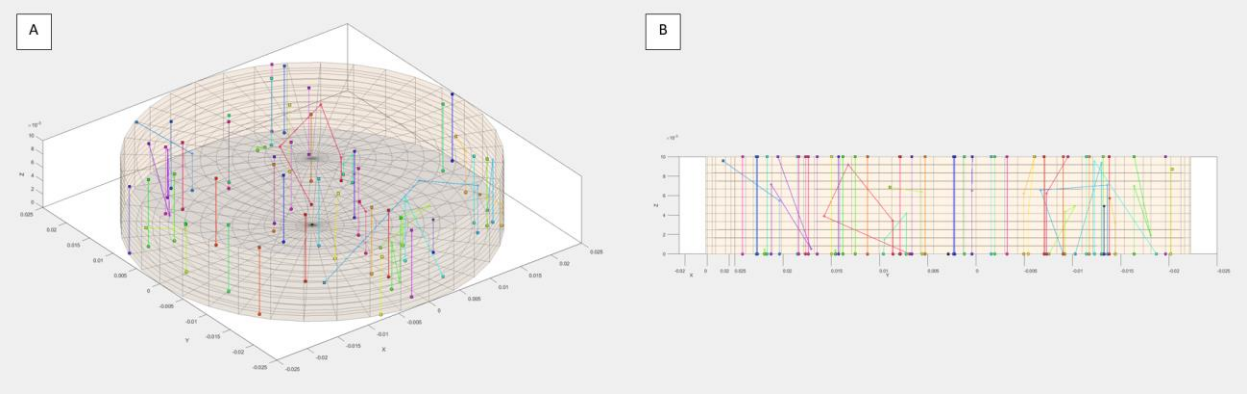

Figure 1: High-level diagram demonstrating light propagation within a circular aerogel monolith. A.) Isometric-view B.) Side-view. Notable points include light can transmit through the aerogel as well as scatter forwards and backwards out of the aerogel.

A high-level diagram (Figure 1) is included to demonstrate how aerogels interact with light. In the best-case scenario, there would be little scattering within the visible region allowing for more light transmission. Currently, aerogels heavily scatter within the lower wavelength regions, and reducing this scattering can help improve optical clarity within the visible regions of light.

Building on monolithic aerogel synthesis, work done at MIT Department of Mechanical Engineering focused on an aerogel optimized to reduce heat losses while maintaining high solar transparency [5]. In the paper provided by Zhao et al, the recipe as well as the thermal and optical properties of an optimized silica aerogel are provided. Silica aerogel samples with a 30 mm thickness demonstrated a hemispherical solar transmittance of 89% [5] and a thermal conductivity of approximately 0.048 W/(m·K) at 80 degrees Celsius [5]. This paper highlighted how the thermal conductivity of the silica aerogel is dependent on the thickness of the sample. Also, Zhao et al.'s work highlighted the optical behaviour of their silica aerogel within the visual and infrared as being highly transmissive in visible and having some absorption peaks in the near infrared. Here, the focus behind the synthesis of the aerogel was to reduce the amount of scattering while maintaining thermal insulative properties.

Current developments within aerogel synthesis also include the employment of bimetallic nanoparticles within the synthesis process. In a paper authored by Gunes et al. at Uskudar University, the sol-gel method is used to prepare aerogel supported bimetallic nanoparticles (NPs) through polymerization chemistry [7]. The process includes hydrolysis, introduction of metal precursors or NPs, condensation/gelation, solvent exchange, drying, and thermal or chemical treatment. The majority of the synthesis routes utilized TEOS as the precursor with subsequent steps involving solvent exchange, supercritical drying, and conversion of metal precursors to bimetallic NPs through thermal treatment or reduction [7]. The work done by Gunes et al. also included utilizing colloidal nanoparticles within wet-gel synthesis both prior and after the hydrolysis reaction, in both cases requiring filtering, drying and reduction to saturate the aerogel [7].

Similar developments in colloidal dispersion stability were conducted and pathways to nanoparticle-based aerogels were discussed by Matter et al. from ETH Zurich. Here it is mentioned that the optical transparency of the aerogel is strongly connected to the colloidal stability of the nanoparticle dispersion [8]. The difficulty in using dried powders is discussed with mention of agglomeration during the formation of the nanoparticle dispersion based on the polarity of the molecules. For aerogel synthesis, stability of the nanoparticle dispersion is based on the type of solvent used [8]. With homogenous gelation being preferred for monolithic bodies, the main guiding parameters discussed were dispersion concentrations and attraction strengths [8]. For synthesis of monolithic nanoparticle infused aerogels, the concentration of the nanoparticle dispersion needed to be high enough such that it overcame the gravitational and mechanical issues that could occur during gelation (i.e. clustering or settling), with increasing particle size requiring a larger volume fraction [8]. One of the key takeaways being the high mechanical fragility of nanoparticle-based aerogels.

With respect to nanoparticle infused silica aerogels / ambigels (ambiently dried aerogels), Jung et al. reported some interesting work on hybridizing silica aerogels with SiO_2 nanoparticles through ambient drying. Here, the silica aerogels were synthesized using a hydrolysis and polycondensation process with TEOS as the precursor and methanol as the solvent. SiO_2 nanoparticles were added to the solution after the hydrolysis reaction and stirred for 12 hours. After the soaking procedure, the final gel was dried at 150°C for 2 hours and then at 200°C for 2 hours under ambient pressure. Different weight percentages of SiO_2 nanoparticles ranging from

0-0.025 wt. % were used, with larger weight percentages consequentially increasing the gelation time [9]. From their work, it was concluded that with the increase of wt.% of SiO_2 nanoparticles, the thermal conductivity of the sample also increased.

1.3 Overarching Goals and Research Gap

The overarching goal of this thesis is to improve optical and thermal performance of aerogels for optothermal applications. More specifically, the research gap is to find a balance between transmittance in the infrared and visible regions and thermal conductivity with a focus on maintaining visible clarify. Methods to reduce thermal conductivity by increasing infrared absorption while maintaining visible transmittance were investigated. To achieve this, an original approach based on the addition of suspended nanoparticles during the sol-gel synthesis was introduced, and the resulting effect of nanoparticle addition on the optical and thermal properties was measured.

1.4 Project Objectives

The project encompasses the overarching goal that translates into specific objectives defining its success. These project objectives can be summarized as follows:

1.) Determine a viable method for incorporating nanoparticles into silica aerogels while ensuring monolithic integrity, optical clarity and insulative properties.

2.) Measure and compare the hemispherical and direct spectral transmittance of the nanoparticle infused aerogel sample to the pure SiO_2 samples.

3.) Measure and compare the effective thermal conductivity of the nanoparticle infused aerogel sample to the pure SiO_2 samples.

1.5 Thesis Outline

This work, defined by the goals and objectives, deals with the synthesis and optothermal characterization of pure and nanoparticle infused silica aerogel monoliths. This thesis will go

through the fabrication procedure of the synthesized aerogels and will discuss the optical and thermal results. As the silica aerogel processing technique seems to be the first of its kind, there remains room for optimization and extension to applications beyond opto-thermal technologies.

Chapter 2 provides an overview of the theory and background related to aerogels. It introduces the several types of aerogels and discusses the synthesis techniques for transparent aerogels. The limitations of aerogels, such as their fragility and manufacturing difficulties, are mentioned. The various drying techniques employed in aerogel fabrication are explored. The chapter also delves into existing silica aerogel TMOS recipe variations and their specific characteristics. Additionally, the radiative transport through aerogels is discussed in relation to their optical properties.

In Chapter 3, the experimental methodology for fabrication used in the research is detailed. The setup of square and circular sample molds for aerogel fabrication is described. The modified manually controlled autoclave (Manuclave) used for supercritical drying is explained, along with the fume hood setup. The testing procedures, including the specific measurements and techniques employed, are outlined.

Chapter 4 focuses on the fabrication of pure silica aerogel monoliths. The specific recipe and wet chemistry used for silica aerogel synthesis are described, along with the drying procedure using supercritical conditions. The handling and storage procedures for silica aerogel samples are outlined, emphasizing the importance of proper handling to preserve their structural integrity.

Building upon the fabrication techniques discussed in the previous chapter, Chapter 5 explores the fabrication of nanoparticle-infused silica aerogel monoliths. The selection of nanoparticles and their incorporation into the silica aerogel matrix are detailed, highlighting the potential effects of nanoparticles on the properties of the aerogels.

The optical characterization of the fabricated aerogels is the focus of Chapter 6. The spectrophotometry technique used to measure the hemispherical and direct transmittance of the aerogel samples is explained. A simple numerical model of radiative transport is presented, with a specific focus on Rayleigh scattering and brief mention the optically thin regime.

Chapter 7 delves into the thermal characterization of the aerogels, particularly the measurement of their thermal conductivity. The modified guarded hot plate method used to determine the effective thermal conductivity is described. The results of the thermal conductivity measurements are presented.

In Chapter 8, the discussion and conclusions derived from the research findings are presented. The fabrication processes are evaluated, highlighting the successes and potential improvements. The optical transmittance of the aerogels, as determined through spectrophotometry, is discussed along with the implications of the simple numerical model. The thermal conductivity results are analyzed, providing insights into the effectiveness of the fabricated aerogels as insulating materials. A summary statement is provided, summarizing the key outcomes of the research. The chapter concludes with suggestions for future considerations in the field of aerogel research.

Chapter 2 – Theory and Background

2.1 Introduction to Aerogels

Aerogels are the lightest solid with the lowest density on the planet. Derived from a gel, aerogels are extremely porous and have unique material properties [10]. Depending on the fabrication technique utilized, these materials can be made with tailored density, insulation capabilities and porosity. Primarily, the solid portion of the aerogel consists of silica and/or other inorganic materials. These materials form a unique nanostructured network that consist of nano-sized particles and air, forming a porous structure like a sponge. With the pockets of air being so small (2-100 nm)[11], that various phenomena occur such as light scattering and difficulty for heat to travel through the complicated framework through means such as convection. The most common type of aerogel is the silica aerogel. A transparent and colorless material which is glasslike in appearance, metal like in sound and behaves like a ceramic in terms of heat transfer.

These characteristics give aerogels a wide range of potential applications across various industries. One significant area of use is in thermal insulation, where their exceptional thermal conductivity properties make them ideal for energy-efficient buildings, insulated windows, and high-performance insulation materials. Aerogels are also employed in aerospace and automotive industries for their lightweight and heat-resistant properties. In addition, they find applications in environmental remediation, as adsorbents for capturing pollutants and contaminants. Overall, aerogels have made much progress over the past decade and demonstrated immense potential in areas where lightweight, high-performance materials with impeccable thermal insulation, optical, and adsorption properties are required.

2.2 Types of Aerogels

Depending on how they are produced, different compositions of aerogels exist ranging from carbon, polymer, metal oxide to silica aerogels. Carbon aerogels are composed mostly of carbon and are foam like in structure. They are known for their exceptional electrical conductivity, and mechanical strength [12]. As in their name, metal oxide aerogels are made from various metal oxides, such as alumina (Al_2O_3), titania (TiO_2), or zirconia (ZrO_2). These aerogels offer low density and low thermal conductivity [13]. Polymer aerogels are formed by replacing the liquid phase in a gel with a polymer which can be done using different polymerization techniques. These aerogels

can be made from polymers such as polyimide. Polymer aerogels such as polyimide aerogels exhibit properties such as flexibility and inherent hydrophilicity [14]. Lastly, silica aerogels are the most common type of aerogel. They are primarily composed of silicon dioxide (SiO_2) and are known for their extremely low thermal conductivity values while retaining high transparency in the visible spectrum.

Silica aerogels can come in different forms such as monoliths, powders and or films. The powder form allows for easy mixing with other materials, enabling the enhancement of thermal insulation, taking thermal blankets as an example. Silica aerogel films are thin layers of aerogel that can be deposited onto various substrates. These films are often used as coatings. They can provide thermal protection in areas where conventional insulation materials are impractical or cumbersome such as on windowpanes. Monolithic silica aerogel structures can be fabricated into various shapes, such as blocks, panels, or customized forms. Monolithic silica aerogels possess exceptional thermal insulation properties, visible optical clarity, low density, and high porosity.

Beyond the several types of silica aerogel, are silica aerogel post processing techniques. A technique of recent interest embodies annealing the aerogel post drying. During the annealing process, the aerogels are subjected to elevated temperatures for a specific duration, allowing for structural and chemical changes to occur. In terms of optical clarity, annealing can improve the transparency of silica aerogels by reducing light scattering within the material [5]. The high-temperature treatment facilitates the consolidation of the aerogel structure, resulting in reduced porosity and better packing of particles, which leads to improved optical clarity.

2.3 Transparent Aerogel Synthesis Techniques

Various techniques can be employed to synthesize aerogels, including the use of different precursor materials. Some common precursor materials used in aerogel synthesis are TMOS (tetramethyl orthosilicate), TEOS (tetraethyl orthosilicate), MTMS (methyltrimethoxysilane), PTMS (phenyltrimethoxysilane), and MTES (methyltriethoxysilane).

MTMS, PTMS, and MTES are organosilane precursors that can be used to introduce organic groups into the aerogel network. These precursors provide additional functionality and can enhance specific properties of the aerogels such as hydrophobicity and improved thermal stability [6].

TMOS and TEOS are widely used precursors for silica aerogel synthesis. They are hydrolyzed and polymerized to form a gel network, which is then subjected to supercritical drying to remove the solvent, resulting in the formation of a porous aerogel structure. TMOS and TEOS offer good control over the gelation process and allow for the synthesis of highly transparent silica aerogels. Aerogels prepared using TMOS or TEOS are somewhat hydrophilic in nature due to silanol groups that form during hydrolysis [15]. For TEOS, ethanol is used as the co-solvent whereas for TMOS based silica aerogels, methanol is used as the co-solvent.

2.4 Limitations

Silica aerogels, while offering unique properties, have several restrictions that limit their widespread application. One of the major limitations is their fragility, as they are prone to breakage upon impact or mechanical stress due to their low density and porous structure. Manufacturing silica aerogels is also challenging, involving complex and time-consuming processes that require precise control of parameters during gelation, drying, and aging. These difficulties contribute to their higher cost compared to conventional insulation materials, making them expensive. However, ongoing research aims to address these limitations by exploring alternative manufacturing techniques and reinforcing aerogels with composite materials to enhance their durability and impact resistance. Despite their restrictions, the exceptional properties of silica aerogels continue to drive interest and advancements in their production and application.

2.5 Drying Techniques

One of the steps involved in the preparation of aerogels consists of drying post wet gel synthesis. Drying determines the aerogel’s final structure and properties. Various methods have been utilized in the past for drying aerogels such with each their own advantages and limitations. The most common method being supercritical drying, in which the aerogel is exposed to a liquid subjected to an environment at which said liquid reaches its critical temperature and pressure. This allows for the pores to be replaced with the liquid and evacuated during the supercritical phase. This method allows for the preservation of the aerogel's nanoporous structure. Another method is freeze drying, also known as lyophilization, which involves freezing the wet gel and subsequently sublimating the ice under vacuum conditions. This process results in the formation of a porous aerogel structure with minimal shrinkage. Lastly, an approach that has recently come

of interest is subcritical drying and or ambient drying. This process involves slowly evaporating the solvent from the gel at ambient conditions. While this is a quite simple and cost-effective method, it is limited in the sense at which it often leads to shrinkages and cracks. Each drying method offers unique advantages and challenges, with room for improvement depending on the industry being addressed.

2.6 Morphological Characterization Techniques

Aerogels are a nanoporous material which makes it difficult to image the porous structure. Previous studies have investigated porous materials using Micro computed tomography [16]–[18]. These earlier studies emphasized the need for accounting for dual porosity using multiple imaging techniques, such as, micro computed tomography and scanning electron microscopy. Morphological characterization of silica aerogels involves assessing their physical properties at a micro- and nano-scale level. Techniques like scanning electron microscopy (SEM) are commonly employed to visualize and characterize the intricate porous network and surface features of the aerogel. SEM provides high-resolution images that reveal the microstructure of the silica framework. Pore size distribution and analysis is useful influencing the aerogel's thermal and insulating properties. In the case of aerogels, as they have nano pores, imaging using nano computed tomography is required, and it is a non-trivial process due to their fragility [19] it is common practice to freeze the sample prior to imaging.

2.7 Existing Silica Aerogel TMOS Recipe Variations

2.7.1 Baseline Recipe

Although there are many recipes in literature to create silica aerogels, a baseline recipe for TMOS base catalyzed aerogel samples was followed. There are many methods in literature to conduct optimization [20]–[26] of recipes, however, it was beyond the scope of this thesis to conduct a systematic recipe optimization. The general recipe of interest follows the procedure for synthesizing silica aerogels by sol-gel polymerization of tetramethyl orthosilicate (TMOS) using ammonia (NH_3) as the selected catalyst to promote both hydrolysis and condensation reactions. TMOS was diluted by methanol followed by the addition of a solution containing the catalyst ammonia and water. Here, methanol is used instead of ethanol due to methanol’s reaction with methyl groups within TMOS versus ethanol’s reactions with ethyl groups when using TEOS. If

ethanol were used with TMOS instead of methanol, its predicted that transesterification and inconsistent trends would occur similar to when methanol is added to TEOS [27]. Then, the solution was left to gel in a mold and sealed with a parafilm sheet. After a set time (ranging from 30-60 minutes), dependent on the precursor, dilutant and catalyst, the lid of the sol-gel mold is removed. This is followed by addition of methanol on the surface layer of the gel and kept submerged in a methanol reservoir / bath to be cycled with fresh methanol after 24 hours for 2 days. The initial solvent (MeOH) is then replaced with ethanol (EtOH) and the ethanol is then cycled every 24 hours for 3 days to be prepared for critical point drying as EtOH is miscible with liquid CO_2. The gel is then super-critically dried. A high-level depiction of silica aerogel synthesis can be shown in Figure 2.

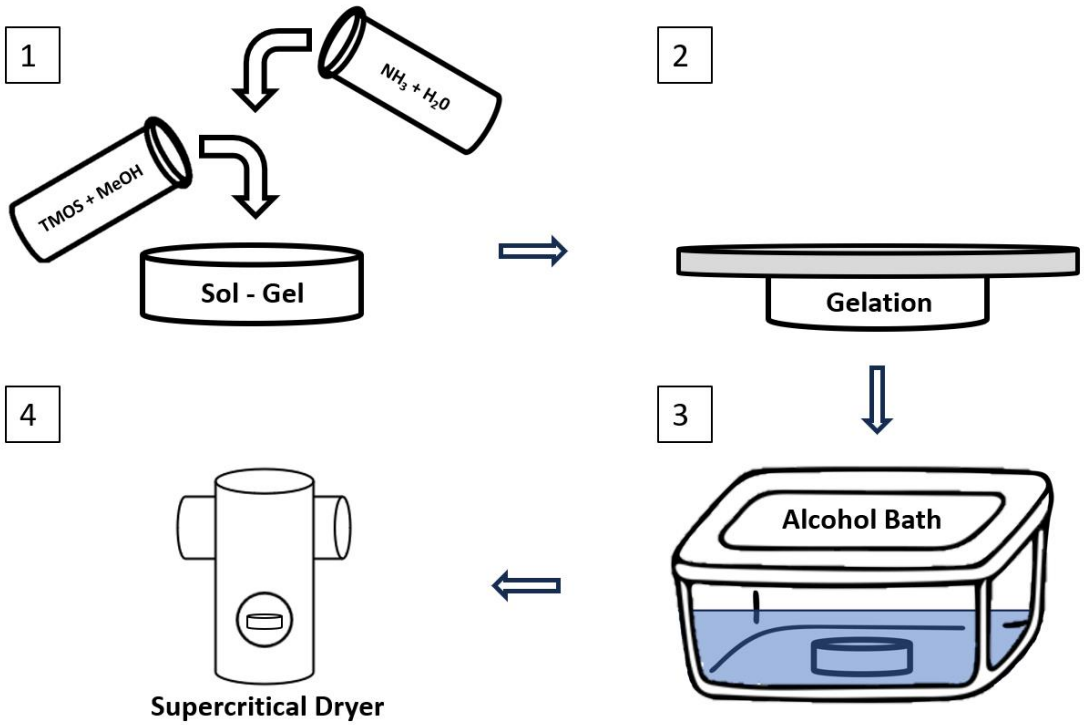

Figure 2: High level diagram of the fabrication steps for silica aerogel synthesis. 1.) wet chemistry, 2.) Gelation, 3.) Solvent exchange / alcohol bath, 4.) Supercritical drying

2.7.2 University of Bath (UOB) *Silica Aerogel Recipe*

A recipe developed by Michael Grogan at the university of Bath followed the same general recipe for procuring silica aerogels (Figure 3) with the use of tetramethyl orthosilicate (TMOS, 218472,

Sigma Aldrich) as the base and ammonium hydroxide solution (NH_4OH 28-30%, 221228, Sigma Aldrich) as a catalyst to promote both hydrolysis and condensation reactions. Then, the solution was gelled in a disposable aluminum container and sealed with a parafilm sheet for 30 minutes to an hour. Following the same basic procedure outlined in 2.7.1 .

Figure 3: TMOS base-catalyzed silica aerogel. University of Bath, UK. Image courtesy Michael Grogan [28], [29].

2.7.3 Massachusetts Institute of Technology (MIT) *Silica Aerogel Recipe*

Massachusetts Institute of Technology followed the same general recipe for procuring silica aerogels (Figure 4) with the use of tetramethyl orthosilicate (TMOS, 218472, Sigma Aldrich) as the base and a more concentrated ammonia solution (NH_3 2.0M in Methanol, 341428, Sigma Aldrich) as a catalyst to promote both hydrolysis and condensation reactions [30]. The solution was gelled in a disposable aluminum container and sealed with a parafilm sheet for 15 minutes. Following the same basic procedure outlined in 2.7.1 .

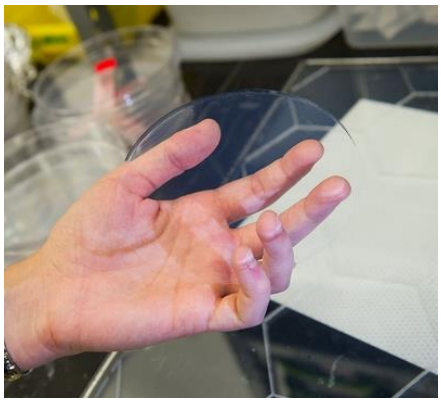

Figure 4: TMOS base-catalyzed silica aerogel. Massachusetts Institute of Technology (MIT), USA. Image taken by Stuart Darsch [31].

2.8 Radiative Transport through Aerogels

The radiative transport equation (RTE) is a governing equation in the field of radiative heat transfer. It describes the behavior of radiant energy as it interacts with participating media, such as gases, liquids, and solids. The RTE quantifies the transfer of energy through radiation by considering absorption, emission, and scattering processes. It considers the directionality and wavelength dependence of radiation and provides a mathematical framework to analyze how energy is absorbed, emitted, and scattered within a medium. The RTE is essential for studying the behavior of radiation within complex systems such as an aerogel. Solving the RTE involves considering the complex interaction of radiation within the silica aerogel framework and can be difficult to approach without some assumptions.

In the optically thick assumption, the thickness of the aerogel sample is sufficiently large compared to the mean free path of light within the material. As a result, light propagates diffusely through the aerogel, allowing for radiative heat transfer to be treated similarly to conduction in terms of equation structure, also known as radiative diffusion. Here, the absorption and scattering processes play a significant role, and the transmittance of the aerogel decreases as the thickness increases.

On the other hand, in the optically thin limit, the thickness of the aerogel sample is much smaller compared to the mean free path of light. In this regime, light encounters minimal scattering and absorption events as it passes through the aerogel. The transmittance is primarily governed by the intrinsic properties of the material, such as its refractive index and absorption coefficient. In the optically thin limit, the aerogel appears more transparent, and its transmittance is high, allowing light to pass through with minimal interactions.

The transition between the optically thick and optically thin limits depends on the specific optical properties of the aerogel, such as its particle size, density, refractive index, and the presence of any embedded nanoparticles. These factors influence the scattering and absorption characteristics within the material, determining the thickness at which the transition occurs. One can determine if the aerogel is within these regimes based on the optical thickness defined in Equation 1.

$$t_o = B_\lambda \cdot s \quad (1)$$

Where t_o is the optical thickness, B_λ is the spectral extinction coefficient and s is the thickness of the sample. A material is considered optically thick if $t_o \gg 1$ [32] and optically thin if $t_o \ll 1$. For the sake of this work, the aerogel will be considered optically thick if $t_o \geq 5$ and optically thin if $t_o \leq 0.25$; otherwise, it will be considered intermediate optical thickness.

Due to the potential dependence of scattering within aerogels based on their optical thickness, different scattering types can be considered: Mie scattering and Rayleigh scattering. Mie scattering occurs when the size of the scatterers (e.g., nanoparticles) is comparable to the wavelength of light. In this case, the scattering behavior is governed by complex interactions of light with respect to the particles of similar or larger size. Rayleigh scattering, on the other hand, occurs when the size of the scatterers is much smaller than the wavelength of light. In this scattering theory, light is scattered with inverse proportionality to that of wavelength to the fourth order. Meaning that smaller wavelengths scatter more than larger wavelengths. The scattering behaviour of aerogels is predominantly influenced by Rayleigh scattering [33], because of this, only Rayleigh scattering will be considered in this work.

Chapter 3 – Experimental Methodology for Fabrication

The experimental design methodology involved the optimization and utilization of a manually controlled autoclave, known as a manuclave, to super-critically dry base and nanoparticle-infused silica aerogels combined with the creation and usage of custom aluminum molds. Post wet chemical synthesis, the solution was poured into the square aluminum molds, covered with parafilm, and left to cure. The gel-filled molds were then loaded into the manuclave. The manuclave provided a controlled environment where pressure and temperature were regulated. This manual control allowed for precise adjustments to create the conditions necessary for supercritical drying. By regulating the pressure and temperature within the manuclave, the solvent was efficiently removed from the gel matrix while maintaining the structural integrity of the aerogels.

3.1.1 Square Sample Molds

To measure the thermal conductivity of silica aerogels using the guarded hotplate method, square aluminum molds were machined to fit the existing apparatus at York University. This allowed for precise and consistent measurements. The fabrication process resulted in the creation of square aerogel samples with dimensions of 40x40 mm and a depth of 6.35 mm. However, during the initial stages, the square molds presented a challenge with mechanical stress concentrations, particularly at the corners where screws were attached. Where due to changes in temperature, the mold would expand and contract, causing stress on the contained aerogel. This led to cracks forming in the aerogel samples as seen in Figure 5. To overcome this issue, a solution was implemented by removing the screws from the molds prior to placing them into the manuclave (Figure 6). This modification effectively eliminated the stress concentration points, ensuring the integrity and quality of the aerogel samples during the thermal conductivity measurements. Additionally, different gaskets were employed to ensure that the aerogels rested properly in the square aluminum molds, ultimately utilizing soft polytetrafluoroethylene (PTFE) as the final selection. PTFE was selected due to its nonreactivity during supercritical drying and hydrophobicity to easily detach from the sample post drying. The square molds were also cleaned using an ultrasonic bath post drying for its next cycle of aerogel synthesis. The ultrasonic drying was useful for ensuring no residual nanoparticles or aerogel specs remained on the mold. This was done by utilizing HPLC water and soap, for 30 minutes in low frequency cleaning for larger

more rough cleaning, followed by just HPLC water for 1 hour in high frequency cleaning for more thorough and intricate surfaces such as the screw holes.

Figure 5: First square (40x40 mm, 6.35 mm♪) base SiO_2 aerogel sample following MIT recipe. The cracks noticeable on the corners of the sample are due to stress concentration points caused from the aluminum mold as well as the PTFE gasket.

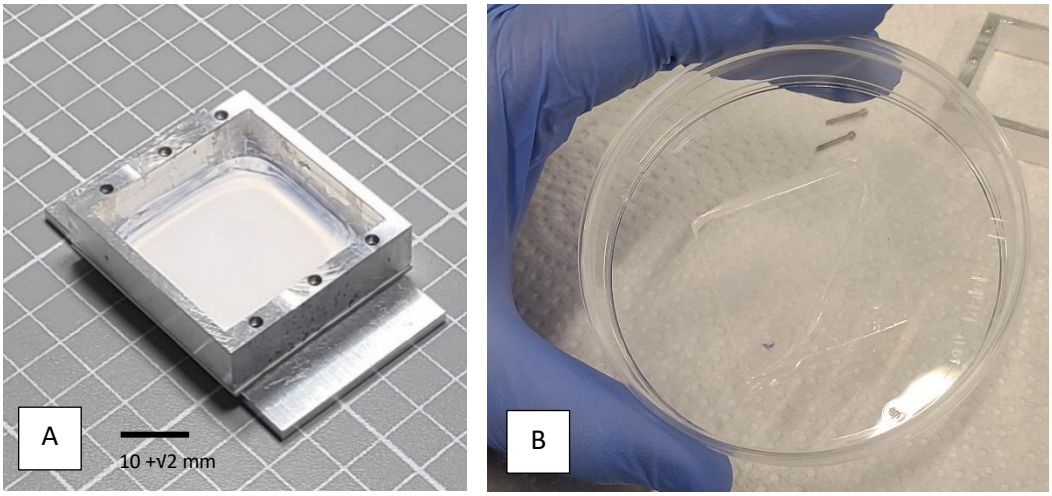

Figure 6: Square (40x40 mm, 6.35 mm♪) base SiO_2 monolithic aerogel sample following MIT recipe. A.) Isometric-view in square aluminum mold, the white base being the PTFE gasket B.) Top-down view. This sample did not have stress concentrations at the corners due to the screws of the mold being remove prior to supercritical drying.

3.1.2 Circular Sample Molds

Initially, circular molds were employed to create silica aerogel samples, serving both aesthetic and practical purposes for repeatable optical measurements. These molds were specifically designed as 40 mm in diameter aluminum sheet punches. The utilization of circular molds significantly expedited the manufacturing process, as it was possible to accommodate up to three

molds simultaneously within the manuclave. This tripling of throughput increased the efficiency of aerogel fabrication, allowing for a higher volume of samples to be produced in a shorter amount of time. The circular molds proved to be a valuable tool in streamlining the manufacturing process while ensuring consistent and reliable results for optical measurements.

3.1.3 Super Critical Dryer: Modified Manually Controlled Autoclave (Manuclave)

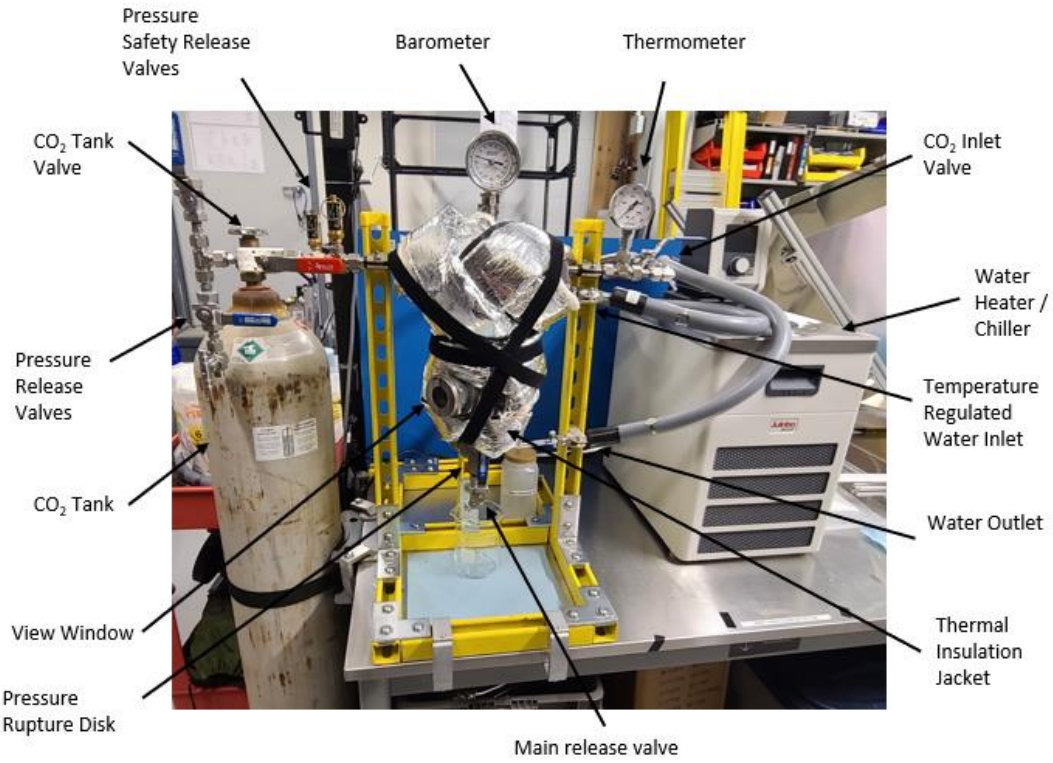

Figure 7: Custom manuclave designed with respect to aerogel.org instructions for drying silica aerogels. [34].

The setup of the supercritical dryer, also known as the manuclave, involved several key components and features to facilitate the drying process of silica aerogels. The manuclave incorporated a window, providing a convenient means to observe the sample and liquid CO_2 levels during the earlier stages of the drying procedure. To protect the surface of the sample from CO_2 droplets, a metal mesh was placed above the mold before inserting it into the manuclave. Temperature control of the manuclave was achieved using a Julabo CD-600F water heater and chiller system, with a temperature-regulating line wrapped around the manuclave. Insulation

played a vital role in maintaining temperature stability, with two types utilized: melamine foam and an aluminum insulation jacket. The window was securely sealed by wrapping nickel Teflon around the thread multiple times (4-5 times). For the CO_2 supply, the tank was equipped with a liquid siphon mechanism that directly pumped liquid CO_2 into the manuclave; special notice was given to the pressure variations caused by the ambient temperature to the tank during drying. The pressure release valves played a crucial role in regulating the CO_2 pressure throughout the different stages of the drying process, including pressurization, supercritical drying, and depressurization (further explained in section 4.1.3). The main release valve facilitated the removal of materials such as liquid ethanol and mixed CO_2 with ethanol from the manuclave. Additional valves were incorporated into the “pressure release” section (as seen in Figure 7) to prevent the formation of ice, ensuring consistent pressure release. The temperature and pressure were regulated to bring the liquid CO_2 into supercritical explained further in section 4.1.3 . This modular design of the manuclave allowed for a controlled and efficient drying process, accommodating the specific requirements of silica aerogel production.

3.1.4 Fume hood Setup

In the laboratory, a well-equipped fume hood was essential for conducting experiments involving silica aerogel synthesis. The fume hood provided a controlled environment for handling chemicals and ensured the safety of researchers. Within the fume hood, a vacuum desiccator was utilized without desiccant for the storage of aerogels. This sealed container created a near vacuum environment, preventing moisture from affecting the aerogels' properties. Bins were strategically placed within the fume hood to facilitate the disposal of used pipette tips, ensuring proper waste management following the safety data sheet (SDS) and maintaining a clean workspace. Various containers, such as beakers and pipettes, were used to hold and transfer the necessary chemicals during the synthesis process. Alcohol baths, a key component in the aerogel synthesis, were also stored and exchanged in designated containers within the fume hood. This setup allowed for easy access to the required materials while maintaining a safe and organized workspace. The fume hood played a crucial role in ensuring proper ventilation and containment of hazardous fumes, creating a controlled environment for wet chemistry experiments involving silica aerogels and the respective nanoparticles used.

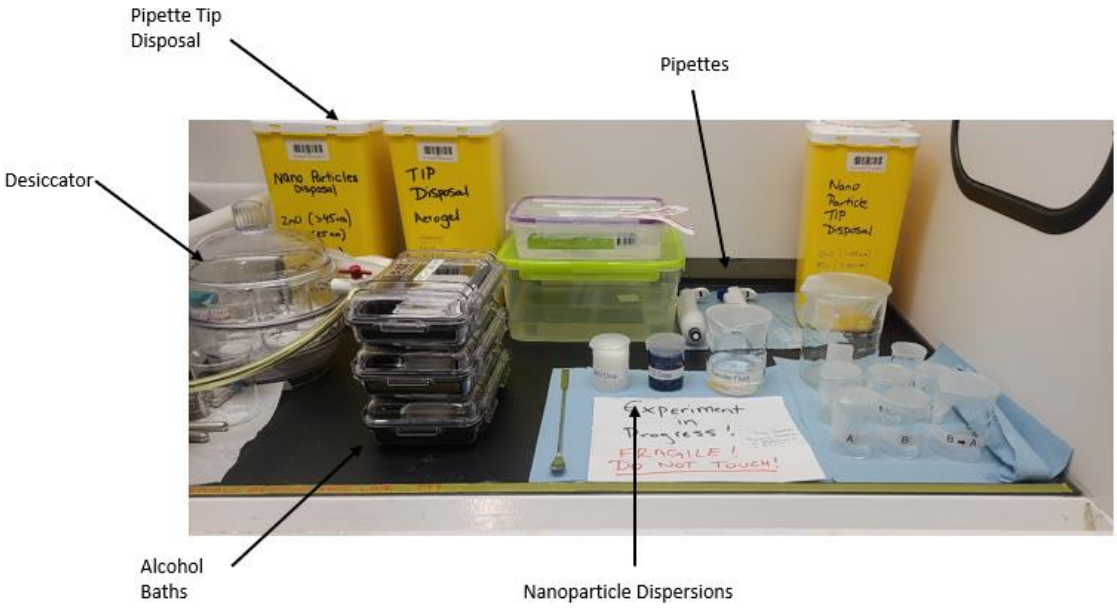

Figure 8:Wet chemistry fume hood setup.

3.1.5 Testing Procedures

3.1.5.1 Mold leak testing

In the process of aerogel production, it was crucial to ensure the proper sealing of the molds to achieve the desired gel thickness. Given the low viscosity of ethanol, thorough testing of the PTFE gaskets and aluminum molds for leaks was essential. To perform the leak tests, the sealed molds were placed on top of tissue paper, and ethanol was carefully poured into the molds. After a 30-minute period, the levels of the ethanol were examined. This procedure helped identify any leaks that could compromise the gel formation and thickness. The selection of suitable gaskets played a critical role in this process, as the aluminum molds alone did not provide sufficient sealing. Choosing a compatible gasket material that could effectively seal the molds and withstand the conditions of the supercritical dryer was of utmost importance in ensuring successful aerogel production.

3.1.5.2 Dilution of nanoparticle / stability solution

In the evaluation of nanoparticle dispersions in water, it was essential to determine if the nanoparticles would remain suspended or precipitate out of the solution to ensure that the aerogels synthesized would be homogenous. To conduct this test, the nanoparticle dispersions were carefully mixed and allowed to settle for a week. The objective was to observe if a considerable number of nanoparticles would settle at the bottom of the beaker (greater than 10% volume fraction), indicating poor suspension stability. It was observed that lower concentrations of nanoparticles tended to result in better suspension stability. Therefore, the addition of nanoparticles to water was a gradual process, ensuring that they were added slowly to prevent agglomeration and facilitate proper mixing throughout the solution. These measures were crucial in assessing the behavior of nanoparticle dispersions and achieving desirable suspension characteristics.

3.1.5.3 Aerogel cutting

Various methods were explored to effectively cut aerogel samples into desired shapes. Initially, during the gelation phase after alcohol baths, thin blades were employed to cut the gel samples. While this approach allowed for cutting without completely damaging the aerogel, it often resulted in unpredictable cracks on the cut pieces. As an alternative, scoring the samples proved to be a more viable technique. However, this method presented challenges when working with smaller sample sizes and did not consistently produce clean cuts. Despite the difficulties encountered, these attempts provided valuable insights for the development of improved cutting techniques for aerogel samples in the future.

Chapter 4 – Fabrication of Pure Silica Aerogel Monoliths

The selection of suitable materials played a crucial role in achieving the desired project objectives. The starting point involved choosing a high-purity silica precursor to ensure the formation of a high-quality aerogel network. Factors such as reactivity, availability, and intrinsic properties were considered in selecting the appropriate precursor. The experimental design of the silica aerogel encompassed the optimization of synthesis parameters, including precursor concentration, solvent choice, and reaction conditions, to achieve the desired nanoparticle dispersion and homogeneous gelation.

4.1 York University Silica Aerogel Recipe, Fabrication and Material Selection

The recipe and material selection for the synthesis of silica aerogels involved careful consideration of the choice of precursors and catalysts. Precursors commonly used for silica aerogel synthesis including tetraethyl orthosilicate (TEOS) and tetramethyl orthosilicate (TMOS) were considered. The selection criteria for the precursors were based on factors such as reactivity, gelation time, thermal conductivity, and pore uniformity. TMOS, known for its lower thermal conductivity and uniform pore distribution in aerogels [35], was chosen as the primary precursor due to its widespread use in aerogel synthesis. Additionally, it is hypothesized that the selection of suitable catalysts played a significant role in controlling the gelation kinetics and the resulting microstructure of the aerogels. Basic catalysts, such as ammonium hydroxide (NH_4OH) and concentrated ammonia in MeOH (NH_3 2M in MeOH), were utilized to promote condensation reactions and reduce gelation time [36]. The exposure duration and type of catalyst were carefully optimized to achieve the desired gelation time and gel structure.

4.1.1 Silica Aerogel Precursor

TMOS (tetramethyl orthosilicate) is often chosen over TEOS (tetraethyl orthosilicate) as the precursor for silica aerogel synthesis due to several factors. TMOS offers advantages such as higher reactivity compared to TEOS [35]. The increased reactivity of TMOS enables a more efficient conversion into the silica gel network during the sol-gel process, leading to faster gelation and reduced processing time, where TMOS based catalyzed aerogels gel in approximately 10

minutes versus TEOS based catalyzed aerogels at 3.2 days [35]. This can be advantageous when aiming for improved productivity, shorter synthesis cycles and improved gel homogeneity.

Additionally, synthesis involving TMOS as a precursor provides better control over the gelation process in comparison to TEOS, resulting in the formation of a more homogeneous gel structure [37]. The improved gel homogeneity can allow for enhanced nanoparticle dispersion and uniform distribution within the aerogel matrix depending on the nanoparticle solution used. Without nanoparticle compatibility, agglomeration can occur which is undesirable. Homogeneity is crucial when incorporating nanoparticles into the silica aerogels, as it ensures consistent and predictable properties throughout the material.

When it comes to nanoparticle infusion, the use of TMOS as the precursor with nanoparticle suspensions allows for the incorporation of nanoparticles directly into the silica gel network during the sol-gel process. Due to the ability of TMOS being easily hydrolyzed and condensed [38], nanoparticles can be added into synthesis within the hydrolysis reaction in the form of a suspended solution in water.

In summation, TMOS was selected as the precursor for silica aerogel synthesis, motivated by its reactivity, faster gelation time, gel homogeneity, and the ability to easily tailor the properties of the resulting aerogels. These advantages make TMOS a preferred choice for nanoparticle infusion, as it facilitates the integration of nanoparticles into the silica aerogel matrix, leading to aerogels with potentially enhanced properties and optimized opto-thermal characteristics.

4.1.2 Recipe & Wet Chemistry

4.1.2.1 Sol-Gel Procedure at York University

The following describes this work's current procedure for synthesizing silica aerogels by sol-gel polymerization of tetramethyl orthosilicate (TMOS, 218472, Sigma Aldrich). The aerogel was synthesized using an ammonia solution (NH_3, 2.0 M in Methanol, 341428, Sigma Aldrich) as a catalyst to promote both hydrolysis and condensation reactions (seen in Figure 9).

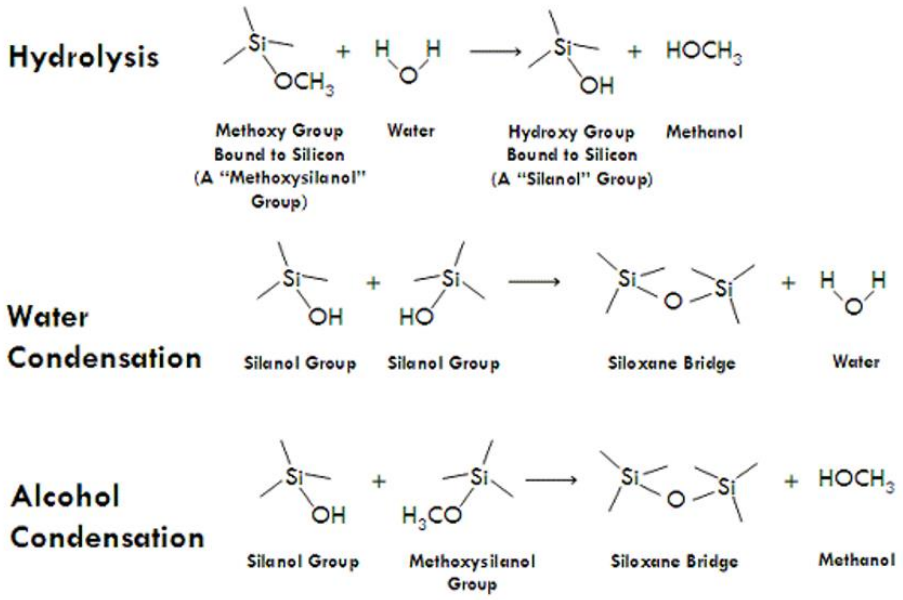

Figure 9: TMOS silica aerogel primary reactions. Hydrolysis produces reactive groups that form polymer links. Both condensation reactions utilize silanol groups to form connective silicon-oxygen-silicon bridges [39].

TMOS was diluted by methanol (MeOH, 322415, Sigma Aldrich) followed by the addition of the ammonia solution and HPLC water (H_2O, 270733, Sigma Aldrich). The mixing molar ratio of chemicals was NH_3:TMOS:H_2O:MeOH = 0.0348:1:4:6.42 [40] (broken down in Figure 10). Here it is important to note that the catalyst is not consumed during the reaction and methanol is noted to have a higher molar concentration as a product due to hydrolysis and condensation.

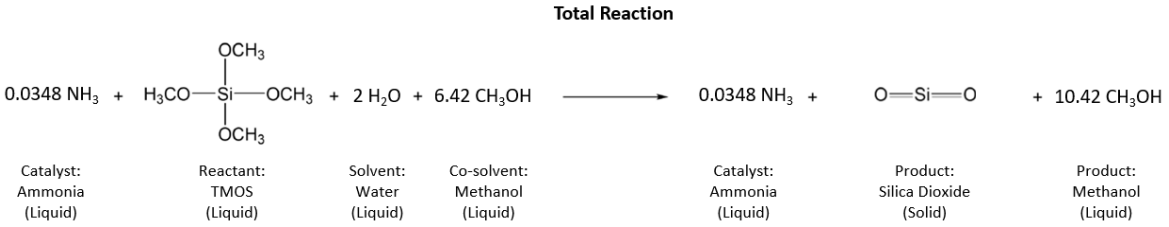

Figure 10: Total reaction chemical formula for TMOS silica aerogel synthesis.

Then, the sol was gelled in a disposable aluminum container and covered with a parafilm sheet. After 30 minutes, the lid of the sol-gel mold was removed, followed by addition of ethanol (EtOH, 818760, Supelco) and kept in an ethanol bath to be cycled with fresh ethanol every 24 hours for 3 days. The initial solvent (MeOH) was replaced with ethanol (EtOH) to be prepared for critical point drying as EtOH is miscible with liquid CO_2. The gel is then super-critically dried in the manuclave following the schematics and procedures taken from Grogan et al.'s methods [34].

The major differences in the followed method include utilizing liquid heating and cooling for the manuclave (as tubing that wrapped around the apparatus) as well as including an insulation jacket around the apparatus as seen in Figure 7. The proposed fabrication alters the recipe such that rather than adding NH_3 and water to TMOS, instead a nanoparticle suspension in water and NH_3 would be added.

Adjustments were made to the fabrication procedure during the sol-gel process. Solutions (ZnO, 721077, Sigma Aldrich / ATO, SN903W, NYACOL® / ZrO_2, ZR20, NYACOL®) were used from varying vendors such as Sigma Aldrich and Nyacol to incorporate unique nanoparticles into the silica aerogels (explained further in section 5.1.1).

In comparison to the recipe used by the University of Bath [28], NH_3 was used in a concentration of 2 M in methanol based on a recipe used in MIT (Table 1), as it resulted in noticeably faster gelation. The timing of gelation was further controlled by exposing the ammonia solution to the environment (air) for a limited period and utilizing it almost immediately after extraction.

The synthesis procedure for the silica aerogels involved the careful mixing and formation of gel solutions. Two separate beakers, labeled A and B, were prepared, and then combined to form the gel solution. Beaker B contained 1.17 mL of NH_3 2M in MeOH and either 4.84 mL of water or a water nanoparticle solution, while beaker A consisted of 10 mL of TMOS and 16.36 mL of MeOH. Beaker B was poured into beaker A. The stirring times were adjusted to 15 seconds due to the rapid curing times associated with the addition of NH_3 2M in MeOH during the procedure. To prevent the formation of bubbles during gelation, a technique was employed wherein the mixture was pipetted onto the side walls of the mold, and any immediately formed bubbles were manually broken with a stir rod. This step was time sensitive as the gel solution gelled within 15 seconds of mixing. To avoid cracking, methanol was applied to the top layer of the gel immediately after removing the parafilm. The samples were then submerged in a mixture of 350 mL of MeOH and EtOH in sequence. Furthermore, the fabrication procedure within the fume hood was optimized to match a whole liquid volume number for TMOS (i.e., 10 ml instead of 10.4 ml), facilitating ease of extraction and safer operating conditions during synthesis. For the creation of the aerogel samples, 10.7 mL of the gel solution was poured into the mold, resulting in samples with a thickness of 6.35 mm and a cross-section of 40 x 40 mm. It was observed that thicker samples, ranging from 1 to 2 cm, exhibited internal cracking.

The decision to choose a thickness of 1/4 inch (6.35 mm) for silica aerogel fabrication was based on its comparability with the industry standard for single-pane windows. This thickness is

commonly used in window applications and provides a practical reference point for evaluating the performance of silica aerogels in terms of thermal insulation and optical properties. By aligning the aerogel thickness with the industry standard, it allows for direct comparisons and potential integration of aerogels into existing window technologies. Additionally, this thickness was found to be within a range that minimized the occurrence of internal cracking, ensuring the structural integrity of the aerogel samples.

Table 1: Similarities and differences between This work, MIT and UOB silica aerogel recipes

Recipe	This work Recipe	MIT Recipe	UOB Recipe
Base	TMOS	TMOS	TMOS
Catalyst	NH_3 2M in MeOH	NH_3 2M in MeOH	NH_4OH in water
Reactant	Nanoparticle dispersion in water	HPLC water	HPLC water
Molar Mixing Ratio	NH_3:TMOS:Water:Methanol = 0.0348:1:4:6.42	NH_3:TMOS:Water:Methanol = 0.0348:1:4:6.42	NH_3:TMOS:Water:Methanol = 0.0031:1:4.122:7.347
Gelation Time	45 seconds	1 minute [30]	8-15 minutes [28]
Drying Method	Supercritical	Supercritical	Supercritical

4.1.3 Drying Procedure: Super-critical

This procedure outlines the steps to dry the silica aerogel samples using a supercritical dryer effectively and safely. Proper execution of this procedure is crucial to obtain high-quality, lightweight, and highly porous aerogels with excellent thermal insulation and optical properties.

The following is a brief procedure for the supercritical drying of silica aerogel samples using CO_2 (detailed procedure can be found in APPENDIX A). Supercritical drying is a critical step in the production of silica aerogels, as it allows for the removal of liquid alcohol and CO_2 from the gel without collapsing its intricate nanoporous structure. The use of supercritical drying allows for the elimination of surface tension, effectively preventing the capillary action that could potentially

damage the delicate aerogel structure. Additionally, this process facilitates the evacuation of alcohol from the silica matrix, leading to the creation of highly porous aerogels. To optimize the drying process, various parameters such as pressures, temperatures, and timings are assessed and adjusted accordingly. It is hypothesized that the rate at which pressure is released, known as the bleed rate, can impact the occurrence of cracking within the aerogel samples. Hence, careful control of the bleed rate is necessary to minimize the risk of structural damage. Moreover, the equalization temperature, which ensures the thermal mass reaches a consistent temperature during heating and cooling, is adjusted considering insulation, environmental conditions, and tank conditions.

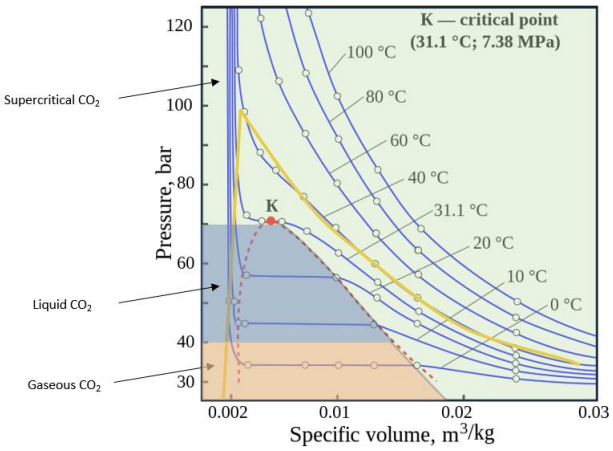

Figure 11: Diagram of CO2 liquid and gas phases as well as supercritical. With the solid yellow line representing the path taken in this work for supercritical drying. The orange section being gaseous CO_2, blue as liquid CO_2, and green as supercritical CO_2. Recreated and modified figure [41].

The sample was placed within the manuclave and sealed tight (86 ft-lbs). Initially, gaseous CO_2 is introduced into the manuclave which is then converted into liquid CO_2 when a pressure of 600 psi and a temperature of 7 degrees Celsius is reached (along with liquid CO_2 also entering the manuclave from the CO_2 tank siphon) as seen in Figure 11. Following this the main drain valve was released for removal of any excess fluids (ethanol) contained in the sample. This step was repeated over 24-hour intervals until no liquid ethanol remained, with the idea that liquid CO_2 replaced the ethanol. This was done by measuring the drained ethanol that exited the manuclave from the main drain in a beaker and comparing it to the initial amount placed within the manuclave. The manuclave was then prepared for supercritical drying by closing all valves then heating and pressurizing the chamber to supercritical. The chamber was kept at around 1400 psi and 40 degrees for 1 hour where the liquid CO_2 transitioned from liquid to supercritical at 31.1 degrees

Celsius and 1070 psi. Pressure was then carefully bled until ambient to allow for the aerogel to be removed safely.

4.1.3.1 Post Drying Remarks

During the post-drying stage of the silica aerogel fabrication process, several observations were made regarding the samples' shrinkage, discoloration, and the formation of craters or frost-like cracks on the surface. These effects were hypothesized to be a result of the interaction between the aerogels and both the liquid and gaseous CO_2 during the supercritical drying process. Additionally, it was noted that stress and pressure changes within the molds caused the aerogels to crack near the corners, particularly in the case of the square aluminum mold. To address this issue, a solution was implemented by removing the screws prior to the drying process, reducing the stress on the aerogels. Furthermore, attempts were made to mitigate cracking by altering the gasket on which the aerogel samples were placed (porous PTFE). These measures aimed to improve the structural integrity of the aerogels and minimize the occurrence of cracks and deformations during the drying phase.

4.1.4 Handling & Storage Procedure

After the supercritical drying process, the storage and handling of silica aerogels required specific precautions. To maintain the desired characteristics of the aerogels, a vacuum chamber or desiccator was utilized for storage, ensuring a vacuum environment. This was essential because exposure to moisture in ambient environments over an extended period could lead to changes in the aerogels' transmittance values, particularly in the infrared (IR) range. Thus, a vacuum storage environment was necessary to preserve pure aerogel characteristics. It was crucial to carefully control the pressurization and depressurization rate of the desiccator since a high bleed rate could cause the aerogels to crack. When handling the aerogel samples, plastic tweezers were used to minimize any potential interference with optical and scanning electron microscope (SEM) results. Additionally, it was observed that aerogels tended to attract dust particles to their surface.

4.1.5 Silica Aerogel Samples

Both the University of Bath (UOB) and Massachusetts Institute of Technology (MIT) recipes were followed to create silica aerogel samples using the existing experimental setup available at York University. Initially, the UOB recipe, following instructions from aerogel.org, was used. The aerogels were synthesized using volumetric proportions and the supercritical dryer. Although this recipe successfully produced silica aerogels, it exhibited a long gelation time and proved to be very fragile. Furthermore, due to the size limitations of the supercritical dryer's inlet, the maximum sample size achievable was 40 x 40 mm. To optimize the throughput using the available aluminum molds, attempts were made to cut the aerogel samples during the gelation state. However, using a blade for cutting resulted in samples with cracks and unpredictable cut patterns (Figure 12).

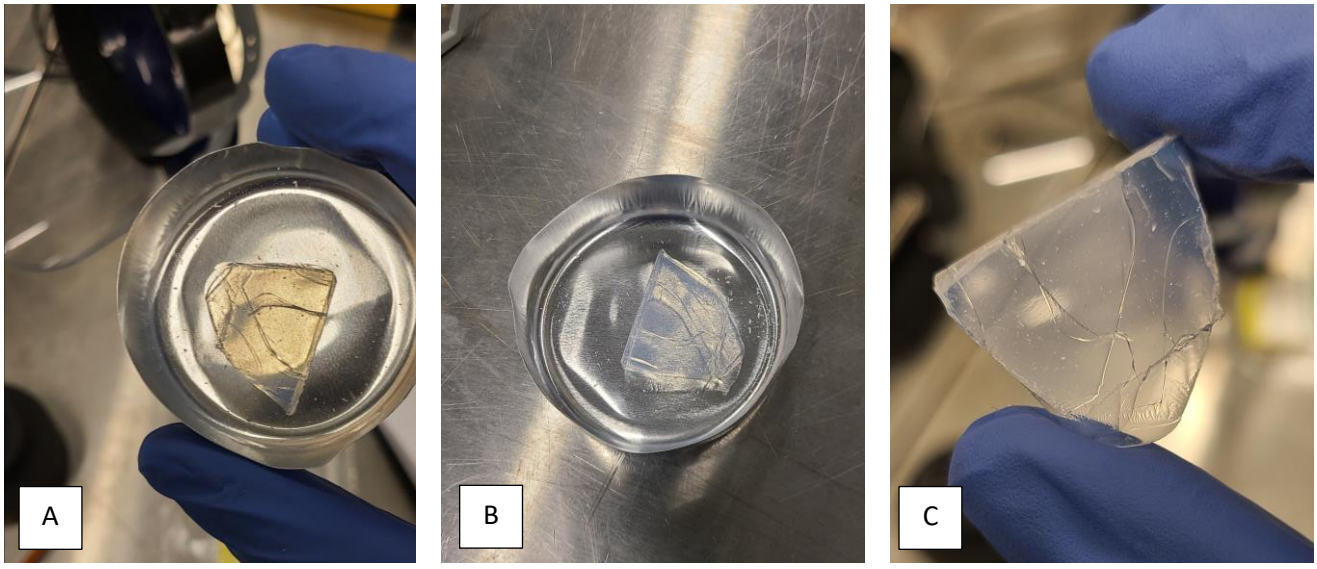

Figure 12: University of Bath (UOB) recreated base SiO_2 quarter circle samples (50 mm Ø, 5 mm ⇃). A.) Top-down view showing the orange color due to reflection of light from the aluminum mold B.) Angled view showing Rayleigh scattering occurring causing the blueish haze C.) Front view of silica aerogel with notably low visible transmittance and cracking due to cutting during wet-gel phase.

Despite these challenges, one sample was successfully created without cracks (Figure 13), although it remained opaque compared to glass. It was observed that slight variations in the volumetric fractions of the catalyst or base in the UOB recipe could hinder gel formation, making it fragile and less suitable for nanoparticle infusion. Therefore, modifications to the concentration of the base (TMOS), catalyst (NH_4OH), or solvent (methanol) would be necessary for successful nanoparticle infusion in the UOB recipe.

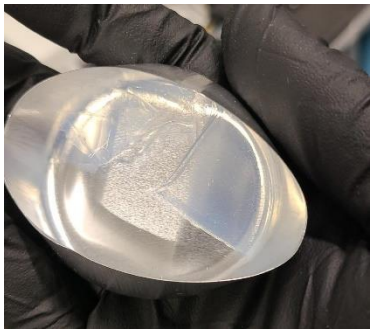

Figure 13: University of Bath (UOB) recreated base SiO_2 crack-free quarter circle sample (50 mm Ø, 5 mm ↓).

To overcome the limitations encountered with the University of Bath (UOB) recipe (such as gelation time and optical clarity), the Massachusetts Institute of Technology (MIT) recipe was explored. In the attempt to replicate the MIT recipe, a different and stronger catalyst, NH_3 2M in methanol, was employed. This modification facilitated faster gelation, addressing the issue of prolonged gelation time observed with the UOB recipe. Another notable distinction was the method of catalyst preparation. In the MIT recipe, the catalyst was initially mixed with methanol, unlike the UOB recipe where it was mixed with water before the wet chemistry process. This difference in preparation method is hypothesized to be considered a contributing factor to the visible clarity exhibited by the resulting aerogel samples from the MIT recipe (results shown in section 6.1.1). The precise ratios between the amounts of methanol, TMOS, and NH_3 used in the MIT recipe played a crucial role in determining the homogeneity, optical clarity, and gelation time of the fabricated aerogels (Figure 14). Notably, with the introduction of the new catalyst, the gelation process occurred instantaneously. However, it was observed that the exposure of the catalyst to ambient conditions after being mixed with water had an impact on its ability to gel.

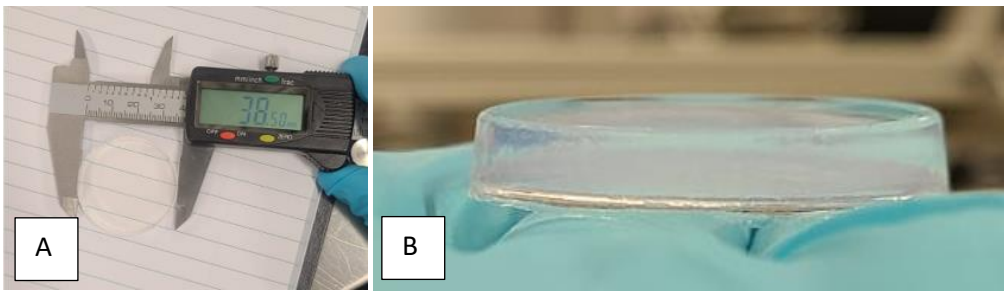

Figure 14: First crack free monolithic base SiO_2 aerogel fabricated at York University following the MIT recipe (38.5 mm Ø, 6.35 mm ↓). A.) Top-down view B.) Side View. Sample shows mild conical shape due to shape of mold as well as the hydrophilic nature of the aerogel (cusp formation)

The MIT base SiO_2 aerogel exhibited several advantages over the UOB SiO_2 aerogel in terms of synthesis and resulting properties. Firstly, the MIT recipe provided a faster gelation time compared to the UOB recipe, allowing for more efficient and streamlined production. The use of concentrated NH_3 2M in methanol as a catalyst in the MIT recipe contributed to the accelerated gelation process. Furthermore, the MIT aerogels displayed comparably improved optical clarity, which is crucial for applications requiring transparent materials. Additionally, the MIT recipe demonstrated better reproducibility, with a higher success rate in producing homogeneous and crack-free samples and with more confidence in successful gelation. These findings emphasize the reasoning behind the selection of the MIT SiO_2 aerogel recipe in terms of gelation time, optical clarity, and reproducibility compared to the UOB SiO_2 aerogel recipe. As the timing of catalyst utilization was a main determinant of gelation time in the MIT recipe, it was deemed highly suitable for nanoparticle infusion purposes.

Chapter 5 – Fabrication of Nanoparticle Infused Silica Aerogel Monoliths

Various nanoparticles were evaluated for their potential to enhance the aerogel's properties. The selection criteria for the nanoparticles included compatibility with the synthesis process, ability to form stable dispersions, and their potential impact on the aerogel's properties, such as optical transmittance and or thermal conductivity.

5.1.1 Nano-particle Selection

The selection process for nanoparticle suspensions used in wet gel synthesis for silica aerogel fabrication was justified based on several considerations. One crucial factor was the choice between water and ethanol as the suspension medium. Water was selected for its compatibility with the sol-gel process and its ability to maintain the stability of the nanoparticles. It offered advantages such as low cost, easy availability, and compatibility with the existing fabrication recipe. Though ethanol, was hypothesized to have superior solubility with certain nanoparticle types and its ability to promote a more uniform dispersion [42], due to uncertainty of its reaction with the existing silica aerogel fabrication recipe, it was not considered. The selection between water and ethanol depended on the specific nanoparticles being used, their surface chemistry, and the desired properties of the resulting aerogels. The selection of the nanoparticle would also serve well to study the effects of scattering and absorption caused by varying nanoparticle size and type within the visible wavelength region. By carefully analyzing the characteristics of the nanoparticles, including their stability and compatibility with the sol-gel process, the appropriate suspension medium could be chosen to ensure the successful synthesis of nanoparticle-infused silica aerogels with desired opto-thermal properties and stability within the aerogel matrix.

5.1.1.1 Zinc Oxide (ZnO)

The selection of zinc oxide (ZnO) nanoparticles for silica aerogel synthesis was driven by its capability to absorb specific UV bands, as demonstrated in its applications in sunscreen.

ZnO nanoparticles possess inherent properties that make them effective in absorbing certain UV bands. Exhibiting a wide bandgap energy, Zinc Oxide nanoparticles can efficiently absorb ultraviolet radiation, particularly in the UV-A and UV-B regions [43].

By leveraging these properties, the inclusion of ZnO nanoparticles in silica aerogels offers the potential for enhanced UV shielding capabilities. The incorporation of ZnO nanoparticles into the aerogel matrix can provide UV protection by absorbing and attenuating specific UV wavelengths, which is beneficial for applications requiring UV shielding, such as in aerospace coatings, UV sensors, or window applications.

Additionally, zinc oxide (ZnO) nanoparticles are a viable option as a water-based suspension for sol-gel synthesis in the fabrication of silica aerogels due to several key reasons. The hydrophilic nature of ZnO nanoparticles (20-40 nm) makes them compatible with water as a suspension medium. Hydrophilicity promotes interactions between the nanoparticles and the water molecules [44], hinting towards stable colloidal suspensions, prevention of particle settling or precipitation during the gelation process and better adhesion towards the gel during wet-gel synthesis. The properties of ZnO nanoparticles such as particle size can be controlled, allowing customization to achieve specific desired properties in the resulting aerogels (larger particle weight percentages of silica leading to larger thermal conductivity [9]).

Here, the ZnO nanoparticle solution (ZnO, 721077, Sigma Aldrich) was diluted using HPLC water (H_2O, 270733, Sigma Aldrich) in low weight percentage at 0.1% with a z-average particle size (mean particle size according to ISO 13321) of 40 nanometers to test how the optical properties in the infrared region are affected, while considering that larger particle sizes affect the opacity of the aerogel in the ultra-violet spectrum [45].

In summary, the selection of ZnO nanoparticles for silica aerogel synthesis is driven by their similar refractive index to pure quartz glass, hypothesizing efficient light transmission, their ability to absorb specific UV bands, demonstrated in applications such as sunscreen, as well as their hydrophilic nature, allowing for solubility within water-based solutions. These properties make ZnO nanoparticles a promising candidate for developing silica aerogels with tailored optical properties and UV shielding capabilities specifically for window-based applications.

5.1.1.2 Antimony-doped Tin Oxide (ATO)

Antimony-doped tin oxide (ATO) nanoparticles were also selected as a nanoparticle suspension to be included in the silica aerogel recipe due to several compelling reasons. Firstly, ATO nanoparticles possess high optical transparency in the visible light range [46], which helps maintain the transparency of the aerogel when incorporated into the matrix. Additionally, ATO nanoparticles exhibit photocatalytic activity [47], allowing for potential future applications in pollutant remediation such as CO_2 carbon capture, and chemical synthesis when integrated into the silica aerogel structure. Lastly, the properties of ATO nanoparticles, such as particle size, and dopant concentration can be tailored to achieve specific desired properties in the resulting aerogels, allowing for customization based on the intended applications.

In summary, the incorporation of ATO nanoparticles as a suspension in the silica aerogel recipe offered the benefits of optical transparency within the visible region, enhanced thermal insulative properties and the ability to customize properties, making ATO nanoparticles an advantageous choice for window applications for optical transparency within the visible region.

5.1.1.3 Zirconia Dioxide (ZrO_2)

Zirconia dioxide (ZrO_2) nanoparticles were an interesting addition for infusion within the silica aerogels recipe. A key factor in the incorporation of zirconia dioxide (ZrO_2) nanoparticles within silica aerogels was their relatively low thermal conductivity. ZrO_2 nanoparticles have a thermal conductivity lower than that of pure silica, which can be beneficial for applications that require efficient thermal insulation. By infusing ZrO_2 nanoparticles into the silica aerogel matrix, the resulting composite material can exhibit enhanced thermal insulation properties, reducing heat transfer and providing improved energy efficiency. This characteristic makes ZrO_2-infused silica aerogels suitable for applications such as thermal insulation & coatings, building window materials, and thermal barriers in various industries, including aerospace, construction, and energy conservation. The combination of ZrO_2 nanoparticles' low thermal conductivity with its other unique structural characteristics makes them a promising choice for enhancing the overall thermal performance and potentially structural functionality of silica aerogels.

5.1.1.4 Nanoparticle Solution Preparation

To create the diluted nanoparticle solution for infusion within the silica aerogel recipe, specific preparations were undertaken. The nanoparticle solution served as a substitute for water in the recipe, with the desired weight percentage set at 0.1%. For the preparation of each nanoparticle solution, meticulous procedures were followed. In the case of Zinc Oxide (ZnO), 0.25 mL of the ZnO nanoparticle dispersion (ZnO, 721077, Sigma Aldrich) was thoroughly mixed with 50 mL of water. Similarly, for Antimony Doped Tin Oxide (ATO), 0.225 mL of the ATO nanoparticle dispersion (ATO, SN903W, NYACOL®) was mixed with 50 mL of water, while for Zirconia Dioxide (ZrO_2), 0.2 mL of the ZrO_2 nanoparticle dispersion (ZrO_2, ZR20, NYACOL®) was combined with 50 mL of water (refer to Table 2 for details). The nanoparticle solutions were all at 20% weight concentrations and were carefully pipetted into a beaker containing 50 mL of water to create the 0.1 wt.% diluted solutions. The mixtures were stirred using a glass stir rod for 2-3 minutes and left to sit for 24 hours to allow any nanoparticles that may have settled to the bottom of the mixture to be identified. These preparations ensured the proper creation of the diluted nanoparticle solutions (Figure 15) used for nanoparticle infusion in the subsequent silica aerogel synthesis process.

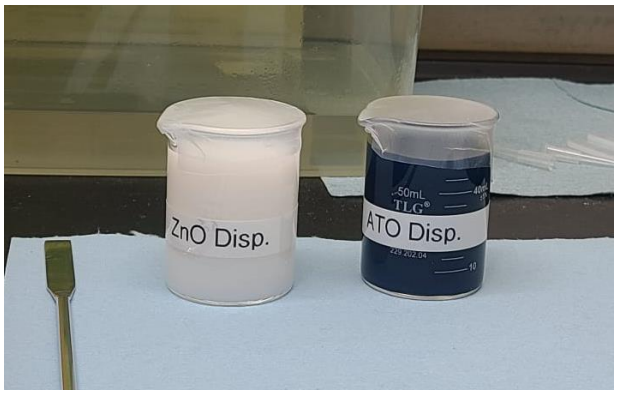

Figure 15: Homogenous nanoparticle ZnO and ATO diluted dispersions in water used in silica aerogel synthesis.

5.1.2 Nanoparticle Infused Silica Aerogel Samples

The concept of infusing nanoparticles into the aerogel matrix initially appeared straightforward, involving the replacement of water either entirely or partially with a nanoparticle suspension.

Exploratory research was conducted to assess the viability of using nanoparticle suspensions in solvents other than water, such as ethanol. However, due to concerns regarding ethanol's reactivity with methanol during synthesis and the impact on the silica structure, water was considered a more time-efficient and lower-risk approach for nanoparticle infusion. Various methods were attempted to incorporate the nanoparticle solution, including variations in weight percentage and volume percentage. Weight percentage was chosen as the preferred approach due to the uncertainties in volume percentages among the different nanoparticle solutions employed. By utilizing weight percentages, parameters such as the volume of dispersion used in the recipe could be kept consistent, allowing for more meaningful comparisons of intrinsic properties, such as density. Additionally, when small amounts of the solution were used (e.g., 0.1 wt. %), the variations in predicted volume percentages were not as significant, making the volume and weight percentages somewhat comparable as notable from Table 2.

Table 2: Nanoparticle diluted solution calculation / setup, where the bulk density of the nanoparticles was a rough estimate allowing for a general sense of the volume percentage.

	ZnO inf. SiO_2	ATO inf. SiO_2	ZrO_2 inf. SiO_2
Molar Mass (g/mol)	81.38	444.23	123.218
Z Average Particle Size (nm)	40	97	20
Nanoparticle Weight (Wt.) % in Dispersion	20%	20%	20%
Measured Density Dispersion (g/mL)	1	1.12	1.26
Dilution Volume Concentration (solute/solvent)	0.50%	0.45%	0.40%
Volume of Dispersion (mL)	0.25	0.225	0.2
Mass Dispersion (g)	0.25	0.252	0.252
Mass Nanoparticle in Dispersion (g)	0.050	0.0504	0.0504
Mass H20 in Dispersion (g)	0.2	0.2016	0.2016
Volume Water Solvent (mL)	50	50	50
Mass Water Solvent (g)	49.9	49.9	49.9
Total Water (g)	50.1	50.1016	50.1016
Nanoparticle Weight (Wt.) % in Diluted Dispersion	0.100%	0.100%	0.100%
Bulk Density Particle (g/mL)	5.61	6.80	5.22
Density of Water (g/mL)	0.998	0.998	0.998
Volume of Particles (mL)	0.008913	0.007412	0.009655
Volume of Water (mL)	50.200401	50.202004	50.202004
Volume %	0.0178%	0.0148%	0.0192%
Measured Volume of Dispersion (mL)	0.05	0.05	0.05
Measured Mass of Dispersion (g)	0.05	0.056	0.063

Nanoparticle infused silica aerogel synthesis was conducted in-house following this works recipe, resulting in the creation of samples with distinct characteristics and properties. Maintaining the same nanoparticle size was attempted but due to lack of availability, the sizes were kept as close as possible while maintaining similar weight percentages. Zinc oxide (ZnO) nanoparticles were initially assessed at various weight percentages. A 0.2 wt. % ZnO infused silica aerogel (Figure 16) was successfully fabricated using a 40 mm diameter circular aluminum mold. The nanoparticle solution was added to the mixture during the sol-gel phase, alongside the catalyst and water. Post supercritical drying, concentrated residual nanoparticles were observed near the center at the bottom of the aerogel. The aerogel exhibited shrinking behavior, with compressive stresses on the top and tension at the bottom. It was noted that thorough mixing of the nanoparticle within the catalyst and water solution prior to the sol-gel phase was essential to avoid agglomeration.

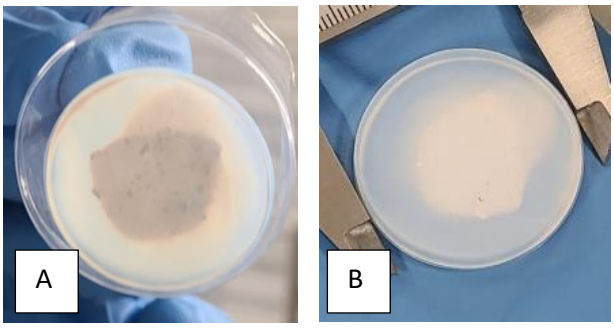

Figure 16: 0.2 wt.% ZnO nanoparticle infused SiO¬2 aerogel (40 mm Ø, 6 mm Ɉ) following the MIT recipe. A.) Bottom view B.) Top view. ZnO particles agglomerated and sank to the bottom near the center of the sample causing a compression and tension forces at the top.

To investigate the impact of nanoparticle type and weight percentage, zinc oxide (ZnO) and antimony doped tin oxide (ATO) were infused into the MIT SiO_2 aerogel recipe at 1 wt. %, resulting in monolithic samples (Figure 17). The ZnO infused aerogel showed lack of optical clarity, particularly within the visible region, while the ATO infused aerogel exhibited agglomeration of nanoparticles near the center, forming cloud like particle structures. With multiple samples being fabricated at once, the success of gelation in the silica aerogel synthesis process was found to be highly dependent on the timing of the catalyst addition. Specifically, when NH_3 2M in methanol was added to water, the duration of exposure of the catalyst to ambient conditions (air) before being incorporated into the solution played a critical role in gelation outcomes. It was observed that longer exposure times often resulted in extended gelation times or even failed gelation attempts. This suggests that the reactivity and effectiveness of the catalyst may be compromised by prolonged exposure to atmospheric conditions, hinting at ammonia escaping into the atmosphere and reducing the effectiveness of the catalyst. Therefore, it is essential to carefully time the addition of the NH_3 2M in methanol to ensure optimal gelation and obtain high-quality silica aerogel samples.

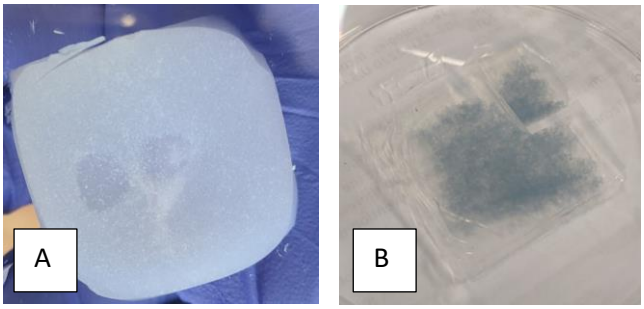

Figure 17: 1 wt.% A.) ZnO top-view B.) ATO isometric-view nanoparticle infused square (40x40 mm, 6.35 mm ⇃) SiO_2 aerogel following MIT recipe. Agglomeration occurred in both samples, more noticeable in B.

By optimizing the recipe with lower weight percentages and using a diluted nanoparticle dispersion as a replacement for water, a successful 0.1 wt. % ZnO infused silica aerogel (Figure 18) with visible clarity and no shrinkage was fabricated. The resulting aerogels qualitatively appeared to have even nanoparticle distribution and successful formation of the silica framework.

Additionally, the fabrication process involved modifications to the drying procedures to enhance the overall quality of the nanoparticle infused silica aerogels. Careful control of the pressure bleed rate during supercritical CO_2 drainage helped minimize the occurrence of cracks and circular popouts on the surface of the aerogels. These imperfections were attributed to inconsistent pressure release and uniform pressure application during the drying process. By optimizing the drying procedures and fine-tuning the aerogel recipe, crack-free aerogel monoliths with improved optical clarity were created.

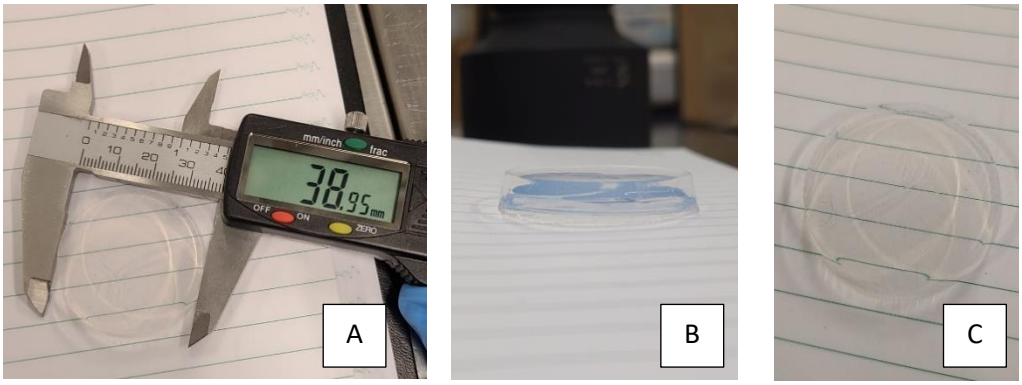

Figure 18: 0.1 wt.% Zinc Oxide infused SiO_2 monolithic circular aerogel following the MIT recipe (39 mm Ø, 6.35 mm ⇃). A.) Top-down view with dimension B.) Side-view C.) Top-down view showing surface finish of sample. Here, the notable circular pop-out is from uniform pressure applied to the sample during super-critical drying.

This work's aerogel recipe led to the fabrication of optically clear and predominantly crack-free nanoparticle infused silica aerogels. Zinc oxide (ZnO), antimony doped tin oxide (ATO), and zirconia dioxide (ZrO_2) aerogel samples (Figure 19) were created following the this works recipe. The visible clarity of the samples followed the trend of ZnO > ATO > ZrO_2, which can be attributed to the specific characteristics and applications of each nanoparticle type. The frost-like texture on the sample surfaces was a result of the interaction between ethanol and liquid CO_2 during the preliminary stages of supercritical drying. When ethanol mixes with liquid CO_2, although they are miscible, the mixture does not react or allow additional liquid CO_2 to permeate the sample until the ethanol mixture is removed from the manuclave. As a result, a frost-like physical formation occurs on the surface, indicating the presence of the ethanol / CO_2 mixture.

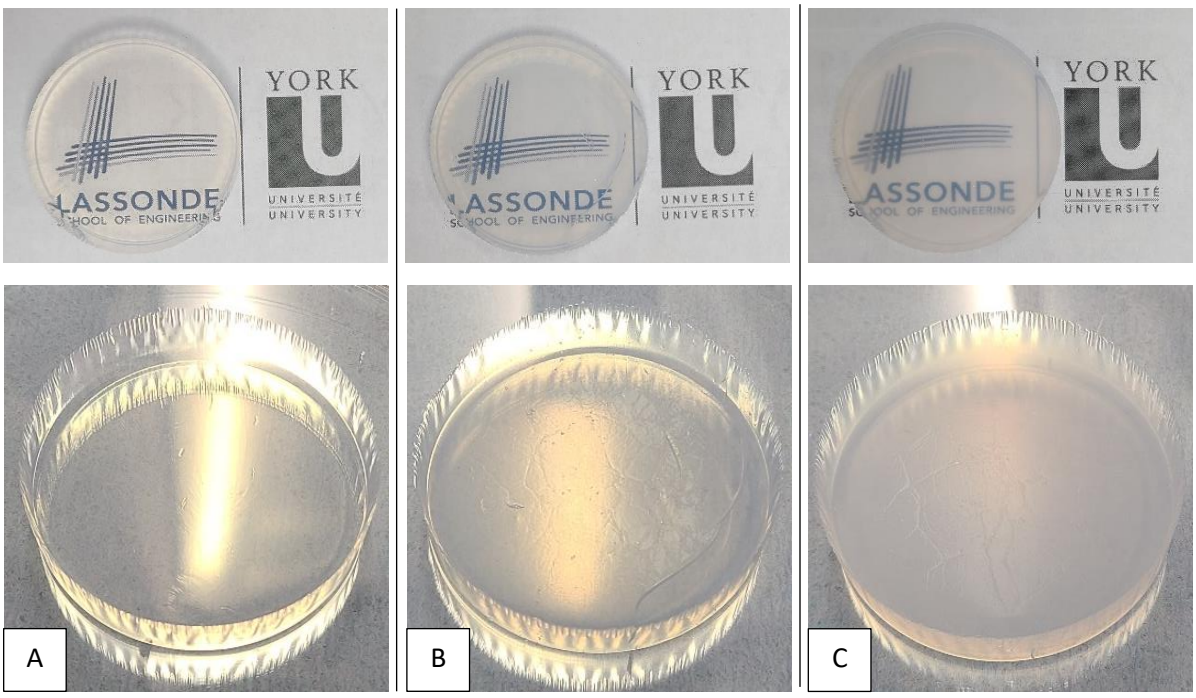

Figure 19: Final nanoparticle infused SiO_2 monolithic circular aerogel samples following the MIT recipe (40 mm Ø, 6.35mm ↓). A.) ZnO, B.) ATO, C.) ZrO_2.

The images captured from the samples (Figure 19) displayed the diffusion of light, indicating the aerogels' ability to absorb and scatter light. This characteristic added to the allure of each unique nanoparticle infused silica aerogel, highlighting the potential for various applications where light manipulation and scattering properties are desirable. The qualitative findings from these experiments underscore the significance of carefully selecting nanoparticle types, optimizing weight percentages, and fine-tuning the synthesis process to achieve desired properties in nanoparticle infused silica aerogels. With this work, the first known nanoparticle infused silica aerogel samples were created at York University to the authors knowledge.

Chapter 6 – Optical Characterization

Optical characterization plays a pivotal role in assessing and optimizing the performance of monolithic silica aerogels, particularly for applications involving windows in commercial or industrial buildings. The unique optical properties of silica aerogels, such as light scattering and absorption, present both challenges and opportunities for understanding their behavior. The presence of random porous structures within the aerogel framework adds complexity to predicting their optical performance. In this chapter, we delve into the transmittance measurements of both pure and nanoparticle-infused silica aerogels. By comprehending the behavior of different aerogels across the visible and infrared spectra, we gain valuable insights for further enhancing their performance through modifications and tailoring of the aerogel recipes. The exploration of optical properties in this study paves the way for advancements in the utilization and design of silica aerogels in window applications.

6.1 Spectrophotometry

Spectrophotometers measure transmittance by sensing the amount of light that passes through a sample compared to incident light shined upon it. The process involves emitting a beam of light with a specific wavelength or range of wavelengths from the spectrophotometers light source. The aerogel sample is placed in a holder which is in the path of collimated light beam, and the light interacts with the sample. Some of the light is either absorbed, reflected and or scattered by the sample's surface and volume, while the remaining light is transmitted through the sample. On the other side of the sample, a light receiver captures the transmitted light. This data is compared to reference data obtained when no sample is present, allowing for a baseline measurement comparison to determine the amount of light transmitted through the sample. Transmittance at different wavelengths (τ_λ) is then calculated as the ratio of the transmitted light intensity (I_t) to the incident light intensity (I_0), expressed as a percentage as seen in Equation 2.

$$\tau_\lambda = \frac{I_t}{I_0} \tag{2}$$

The direct transmittance of SiO_2 aerogel was characterized through spectrophotometric measurements utilizing the Shimadzu UV-2600 Spectrophotometer (UV-Vis) and the Bruker Vertex 70 Fourier Transform - NIR & MIR Spectrometer. These instruments covered wavelength ranges of 200-800 nm and 800-7000 nm, respectively. The experimental setup involved directing incident light towards the aerogel sample, allowing for the measurement of both direct and hemispherical transmittance spectra.

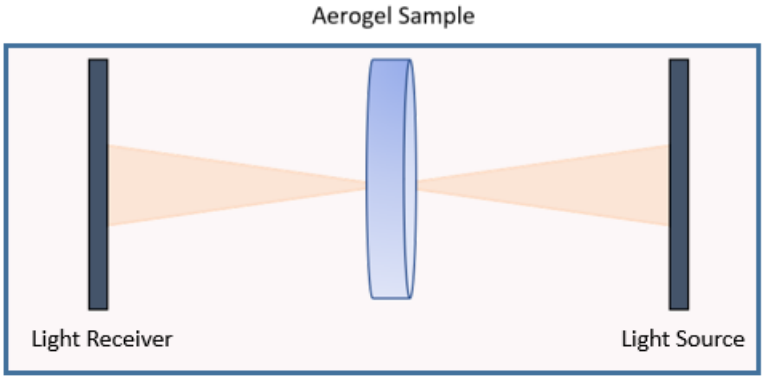

Figure 20: General optical layout setup for direct transmittance measurements in spectrophotometers.

The optical characterization of the aerogel samples focused on the spectral range of 200-7000 nm to assess both visible light and infrared transmittance behaviors. To ensure consistent measurements, efforts were made to maintain the aerogel sample in the same position throughout the tests, allowing the beam of light to consistently hit the same area of the sample during measurements using both the UV-Vis and FTIR spectrophotometers. This approach facilitated repeatable and reliable data acquisition. For each measurement, a 6.35 mm thick aerogel sample was positioned parallel to the incident light, with the detector positioned on the opposite side to capture the transmitted light.

Both hemispherical and direct transmittance values were measured. Hemispherical transmittance (direct + diffuse) was determined using the integrating sphere attachment on the UV-Vis spectrophotometer within the range of 200-1400 nm. Direct transmittance values, on the other hand, were measured using different instruments depending on the wavelength range. The UV-VIS spectrophotometer was used to measure direct transmittance in the range of 200-900 nm,

while the FTIR spectrometer was employed for the range of 800-2500 nm in the near infrared (NIR) setting. For wavelengths spanning 2500-7000 nm, the FTIR spectrometer was utilized in the mid infrared (MIR) setting.

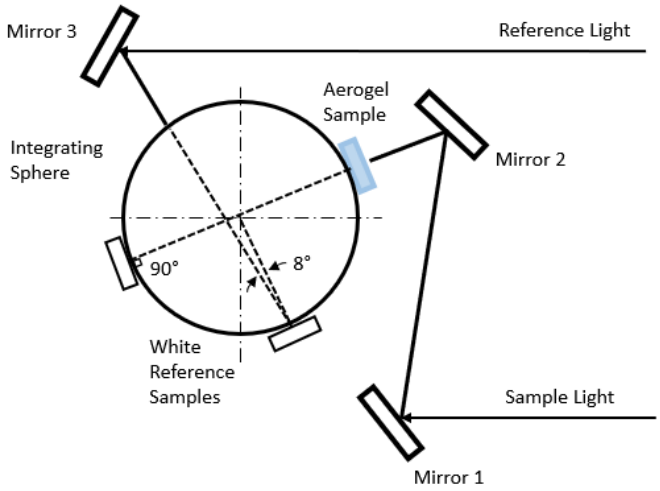

Figure 21: Rough schematic diagram of UV-VIS 2600 integrating sphere setup for hemispherical transmittance measurement of fabricated silica aerogel samples recreated from UV-VIS 2600 manual.

In a study conducted by Zhao et al [5], an experiment was performed to evaluate the direct-hemispherical transmittance of an 8mm thick silica aerogel sample using FTIR-NIR and UV-VIS spectrophotometric measurements. For comparison, visible and IR transmittance values of soda-lime glass were also included in the analysis. The resulting graph (Figure 22) depicts distinctive characteristics of the aerogel's transmittance behavior. Notably, the aerogel exhibits a solar weighted transmittance of 94.8% for a 10 mm thick sample [5], calculated by taking the average transmittance measurements from 300-2500 nanometers (the addition of both hemispherical measurements in visual and direct measurements in near infrared). In the infrared range, between 1 and 3 μm, the graph shows additional peaks that arise from the absorption of water molecules present on the surface of silica particles [5]. It is worth noting that an ideal curve representing a perfect silica aerogel for window applications would exhibit 100% transmittance in the visible region and a gradual decrease to 0% transmittance beyond 900 nm. The diagram serves as a visual reference to illustrate the differences in transmittance measurements between the aerogel fabricated in the related paper and soda-lime glass.

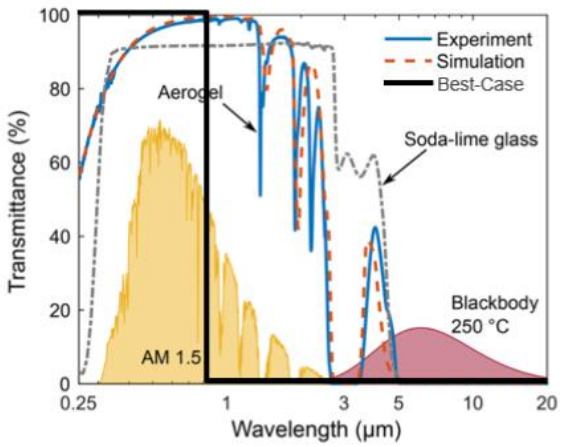

Figure 22: Direct-hemispherical transmittance spectrum of an 8 mm thick aerogel sample. Transmittance of the soda-lime glass slide is shown for comparison. Regions of interest include the silica aerogel experimental transmittance (solid blue line), transmittance of soda-lime glass (dotted grey line) and the best-case silica aerogel for this work's transmittance (solid black line). (Figure included from ACS Nano 2019, 13, 7508-7516 publication)

6.1.1 Hemispherical & Direct Transmittance Measurements

In this study, we conducted direct-hemispherical transmittance measurements on various types of silica dioxide aerogel samples. Specifically, we examined pure silica dioxide aerogel, as well as aerogels infused with Antimony Doped Tin Oxide (ATO), Zinc Oxide, and Zirconia Dioxide. The resulting data (Figure 23) is presented using both dotted and solid lines on the graph. The dotted lines represent the hemispherical transmittance values, which account for both direct and diffuse light. On the other hand, the solid lines represent the direct transmittance values. A recognizable change in the transmittance occurs around 900 nanometers, indicating the transition between the UV-Vis and FTIR measurement apparatus.

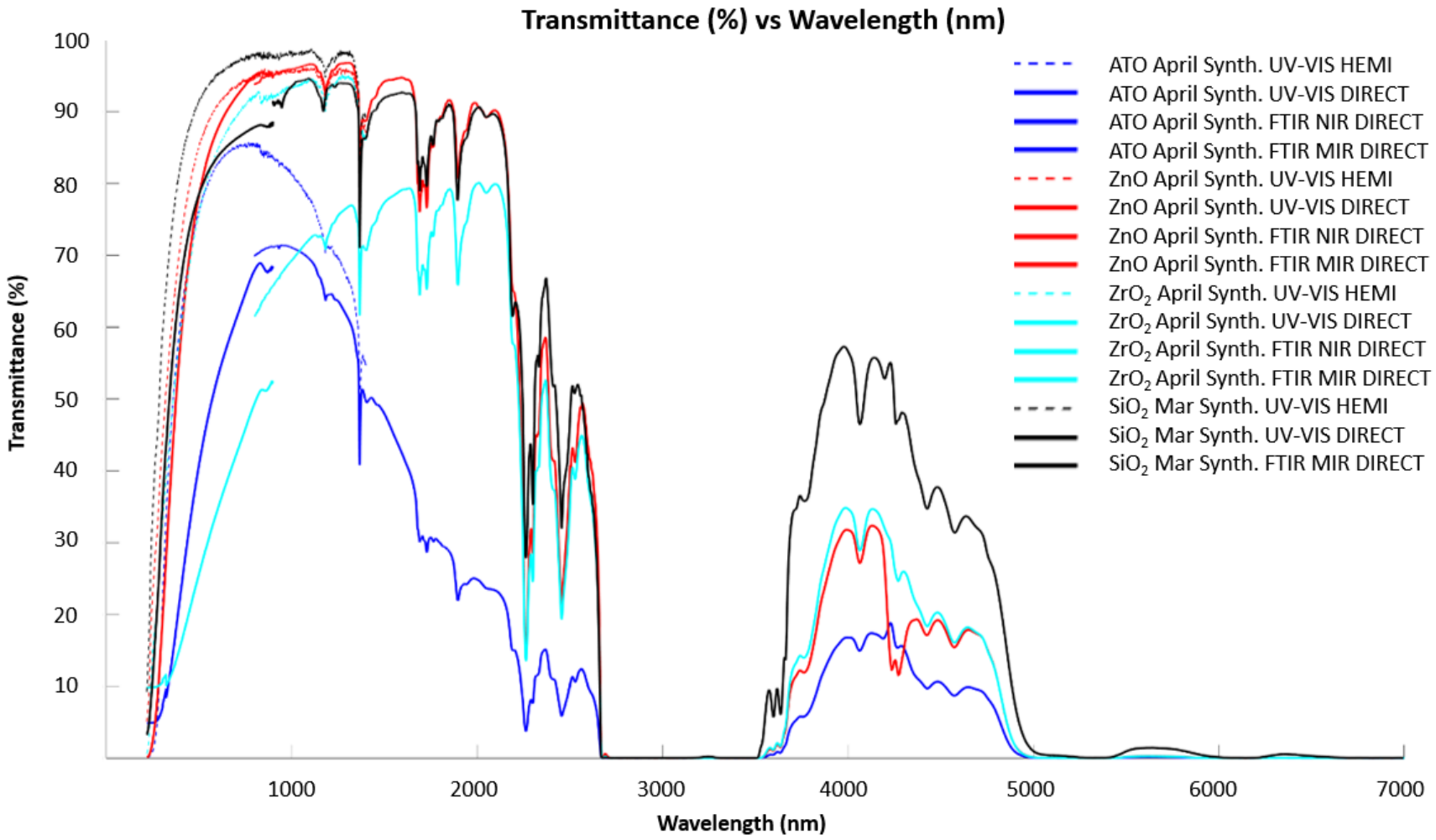

Figure 23: Transmittance percentage comparison of 6.35 mm ↧ and 40 mm Ø aerogel samples

The measured transmittance data reveals two significant regions of interest. Firstly, in the visible spectrum from 380 to 700 nanometers, each aerogel exhibits distinct behavior, demonstrating patterns of scattering and absorption as the transmittance plots gradually reach a plateau. This suggests that the aerogels interact differently with light specifically within the lower wavelength regions, resulting in variations in their optical properties. Secondly, in the range of 3500 to 5000 nm, there is another notable transmission region where the aerogels display their ability to absorb light in the infrared, hypothesized to be due to adsorbed water. Among the three nanoparticle-infused silica aerogels, the zinc oxide infused silica aerogel sample stands out as it follows the desired trends for optimal window applications. It exhibits high transmittance (above 85%) in the visible range while maintaining relatively low transmittance (below 40%) in the infrared spectrum. This characteristic makes the zinc oxide-infused silica aerogel a promising candidate for achieving a balance between visible light transmittance and infrared blocking capabilities, which are desirable qualities for efficient window materials. The solar weighted mean transmittance for each sample was measured by taking an average of the transmittance values from 300-2500 nanometers, where the values from 300-1400 were from hemispherical measurements and the values from 1400-2500 were direct measurements (Table 3). The Zinc Oxide-infused Silica aerogel also performed the best amongst the nanoparticle infused samples in terms of solar weighted transmittance at 85.53%, comparing very closely to the measured pure Silica sample at 86.41%.

Table 3: Solar weighted transmittance values of measured pure and nanoparticle infused silica aerogel samples.

Recipe	Solar Weighted Transmittance (%)
SiO_2	86.41
ZnO infused SiO_2	85.53
ATO infused SiO_2	55.43
ZrO_2 infused SiO_2	77.70

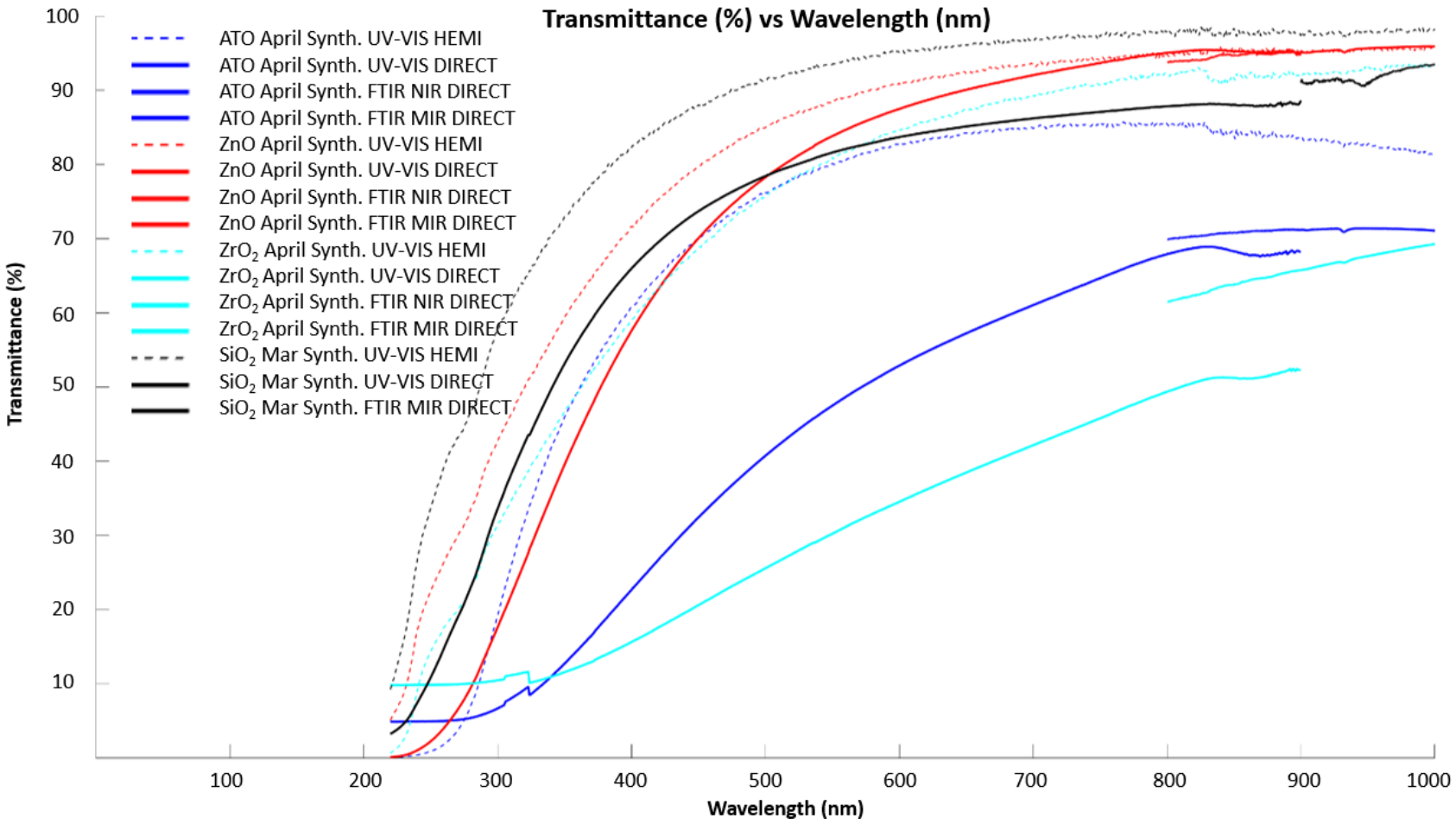

Figure 24: Visible Transmittance percentage comparison of 6.35 mm ↧ and 40 mm Ø aerogel samples using the UV-Vis and FTIR NIR spectrophotometers.

The observed behavior of the nanoparticle-infused silica aerogel samples in the visible spectrum aligns with their respective characteristics. Among them, the ZrO_2 infused Silica aerogel performs the poorest in terms of visible light transmission (high scattering, low transmittance in visible), exhibiting significant scattering. This behavior is related to its effectiveness as a thermal insulator. On the other hand, the ATO infused Silica aerogel lies in the middle, displaying both substantial scattering (in visible) and absorption (in infrared). This is consistent with its known optical coating capabilities, which are successfully applied to the aerogel despite its low weight percentage. In contrast, the ZnO infused silica aerogel demonstrates a best-case behavior with minimal scattering, closely resembling the hemispherical transmittance measurement of the pure silica aerogel sample. This makes it a favorable candidate for achieving a balance between visible and infrared transmittance, aligning with the research goal. Overall, the ZnO infused Silica aerogel sample exhibits desirable characteristics and shows promise for achieving the desired optical properties in terms of both visible and infrared transmittance.

6.2 Simple Numerical Model of Radiative Transport

Aerogels exhibit interesting behavioural patterns within radiative heat transport specifically for their optical properties. Here, the Radiative Transfer Equation (RTE) is relevant to measuring the transmittance of these materials. The RTE encompasses various phenomena such as transmittance, reflection, and absorption, which are essential in capturing and retaining thermal energy within aerogels. Depending on the application, the RTE can be quite complex to solve. In this regard, there can be approaches made to analytically simplify the equation such as considering the sample to be either optically thick or optically thin.

The types of scattering and their relation to the spectral extinction coefficient is also essential when studying the RTE and optical properties of aerogels, especially those infused with nanoparticles. The spectral extinction coefficient (defined in Equation 3) quantifies the combined effects of absorption and scattering, and it can vary depending on the size, shape, and composition of the nanoparticles present in the aerogel matrix.

$$B_\lambda = \kappa_\lambda + \sigma_{\lambda,sca} \tag{3}$$

Where κ_λ is the spectral absorption coefficient and $\sigma_{\lambda,sca}$ is the spectral scattering coefficient.

By characterizing the extinction coefficient, we can approximate the interaction of light with aerogel structure, in particular the optical transparency. In a study by Fricke et.al, it is shown that the optical transparency of silica aerogels is tied closely to its microstructure which acts according to Rayleigh scattering [48].

6.2.1 Rayleigh Scattering

In the case of silica aerogels, Rayleigh scattering occurs when the characteristic size x (defined in Equation 4) of the aerogel's nanoparticle structures is much smaller than the incident light's wavelength. This scattering mechanism leads to the preferential scattering of shorter wavelength light, such as blue and violet, while longer wavelengths, such as red and infrared, experience less scattering.

$$x = \frac{2\pi a}{\lambda} \ll 1 \tag{4}$$

Where a is the radius of the particle and λ is the wavelength of incident light in the medium [49].

When considering Rayleigh scattering in silica aerogels, certain assumptions are made. One of these assumptions is that the scattering particles are non-absorbing, meaning they do not absorb the incident light but only scatter it. Additionally, the Rayleigh theory assumes that the scattering efficiency is inversely proportional to the fourth power of the wavelength (λ^{-4})[48]. As a result, shorter wavelengths are scattered more efficiently than longer wavelengths as seen in Equation 5.

$$\tau = A \times \exp\left(-\frac{B}{\lambda^4} s\right) \tag{5}$$

Where τ is the transmittance, A is the wavelength independent coefficient accounting for surface defects, s describes the thickness of the sample, and B describes the extinction contribution coefficient from Rayleigh Scattering [48].

The spectral scattering coefficient ($\sigma_{\lambda,sca}$) can be calculated based on the Rayleigh-Gans theory:

$$\sigma_{\lambda,sca} = 4\pi^4 \frac{\rho_{ap}}{\rho_{SiO_2}} \frac{d^3}{\lambda^4} \left(\frac{n^2 - 1}{n^2 + 2} \right) \tag{6}$$

Where ρ_{ap} is the apparent density of the aerogel sample, ρ_{SiO_2} is the density of the amorphous silica, d is the diameter of the scattering center and n is the relative refractive index of silica to air[48]. For this work, this Equation 6 is further simplified to Equation 7 as:

$$\sigma_{\lambda,sca} = \frac{c}{\lambda^4} \tag{7}$$

where c is a curve fit coefficient which is a material-property based constant characterized by the complex refractive index, particle radius and number density of particles per unit volume.

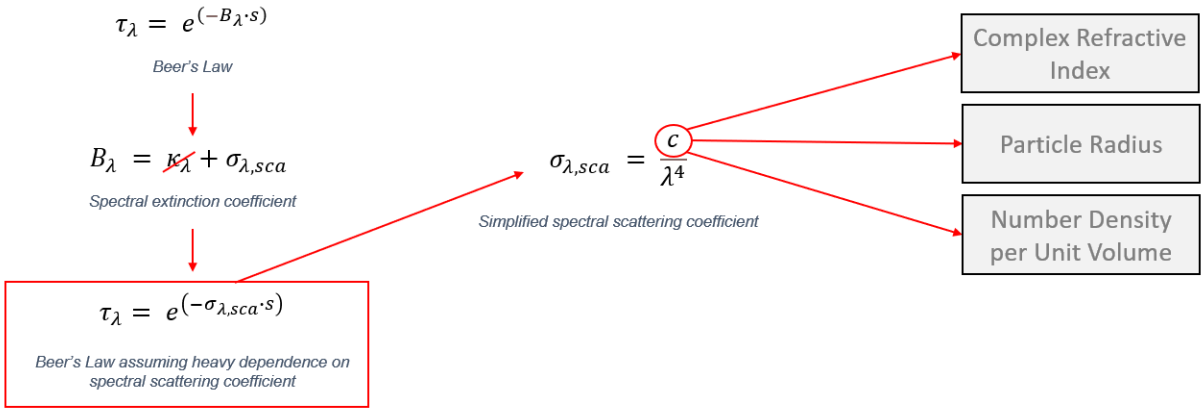

Figure 25: High level summary / breakdown of how scattering was modeled in the simple numerical model.

In summary, the transmittance was modeled with respect to Beer's law, where spectral transmittance was represented by the exponential behaviour of the spectral extinction coefficient and the thickness of the sample. Where the extinction coefficient defines the absorption and scattering properties of radiation within the sample. Based on Rayleigh scattering theory, we can assume that the aerogels will show minimal dependence on absorption during the visible region and focus on the scattering behaviour. Beer's law can therefor be re-written with heavy dependence on the spectral scattering coefficient. The spectral scattering coefficient is determined by a simplified version of Rayleigh-Gans theory, where scattering shows an inverse fourth order relationship with wavelength. Where "c" here can be characterized by the complex refractive index, the particle radius, and the number density per unit volume.

6.2.2 Optically Thin Regime and Beer's Law

When examining the visible region of light, the synthesized silica aerogel samples typically fall within the optically thin regime with respect to Equation 1, where visible light can transmit through the aerogel with ease.

Assuming the aerogel is homogenous, the transmittance of light through the aerogel can be accurately described using Beer's law. Equation 8 states that the logarithm of the ratio of incident light intensity to transmitted light intensity (transmittance) is directly proportional to the sample's thickness and the extinction coefficient.

$$\tau_\lambda = e^{(-B_\lambda \cdot s)} \tag{8}$$

Using the experimental data collected from Figure 23 and the Beer-Lambert-Bouguer equation, the transmittance for the fabricated silica aerogel samples is plotted alongside the theoretical Rayleigh fit transmittance, where it is assumed that the aerogels mainly exhibit attenuation by out-scattering rather than absorption. Allowing the modeled theoretical Rayleigh transmittance to be represented by Equation 9 as

$$\tau_\lambda = e^{(-\sigma_{\lambda,sca} \cdot s)} \tag{9}$$

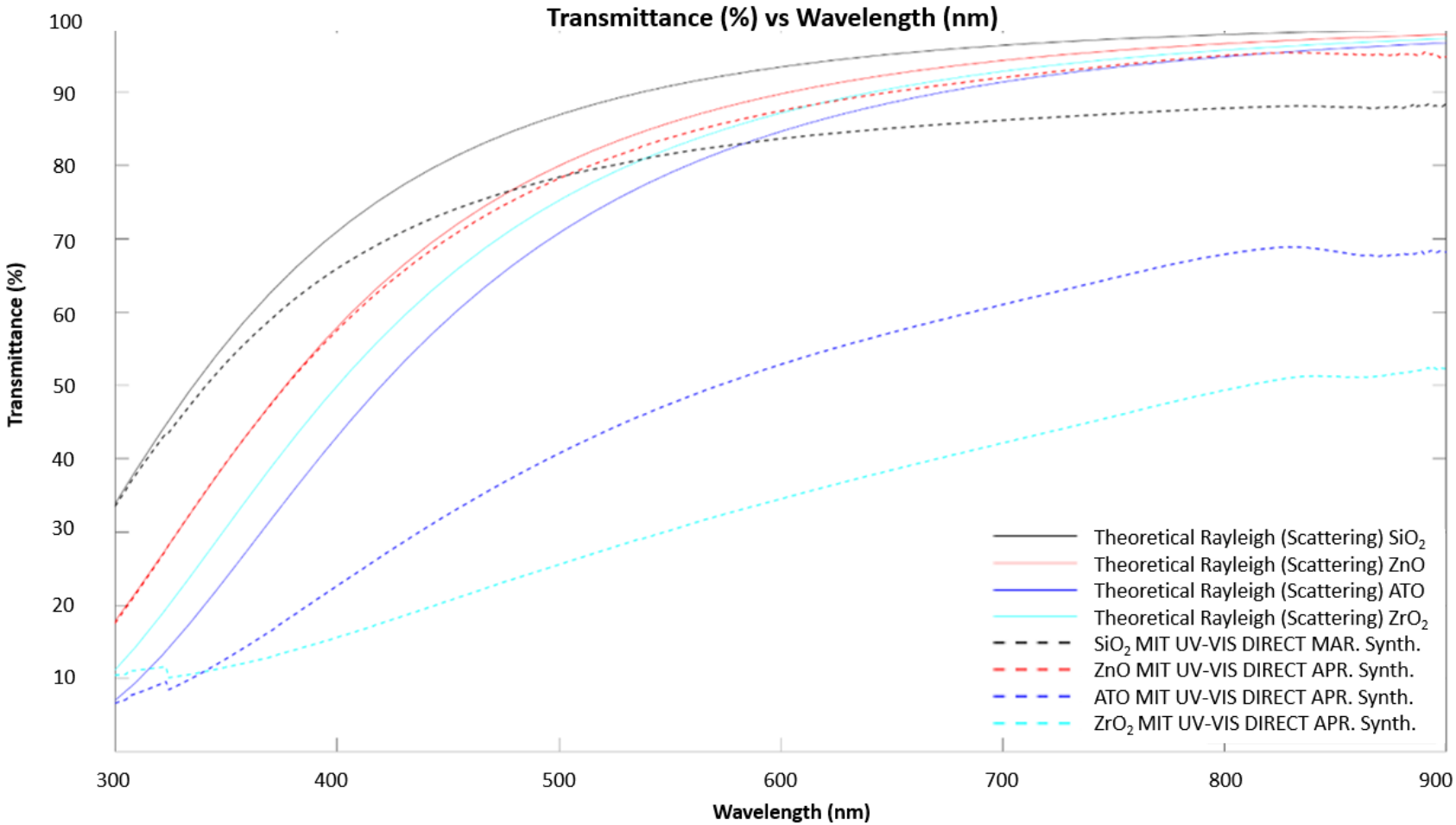

Figure 26: Measured direct spectral transmittance with modeled theoretical Rayleigh transmittance of fabricated aerogel samples.

By utilizing the experimental data obtained through spectrophotometric measurements and the known thickness of the silica aerogel samples, it is possible to determine the extinction coefficient at various wavelengths based on Equation 1. This enables the calculation of the mean optical thickness within the visible region. The direct spectral transmittance values acquired from the spectrophotometers serve as the basis for this analysis.

Table 4: Mean optical thickness per fabricated silica aerogel sample with a thickness of 6.35 mm within the visible wavelength region.

Recipe	Mean Optical Thickness
SiO_2	0.2415
ZnO infused SiO_2	0.2442
ATO infused SiO_2	0.8691
ZrO_2 infused SiO_2	1.2930

The measured optical thicknesses show that SiO_2 and ZnO infused SiO_2 samples fall within the optically thin regime while ATO and ZrO_2 infused SiO_2 samples can be defined as having intermediate optical thickness. This implies that light interacts heavily within the visible region with respect to the thickness of the ATO and ZrO_2 infused silica samples in comparison to pure SiO_2 and ZnO infused silica samples.

Following the measured spectral extinction coefficient values and the modeled theoretic Rayleigh transmittance, the absorption and scattering coefficients were plotted as seen in Figure 27.

Based on this data, it is noticed that after the visible region, the scattering coefficient approaches zero and appears to have little to no effect on the aerogel's extinction coefficient. Specifically, for SiO_2 and ZnO infused SiO_2 since they fall within the optically thin regime, whereas ATO and ZrO_2 infused SiO_2 aerogel samples tend to shift heavily towards the extinction coefficient being based on the absorption coefficient. This means that ATO and ZrO_2 infused Silica aerogels have absorptive properties within the visible region, and this simple numerical model might not be well suited to characterize their respective absorption and scattering coefficients. Here Table 4 can be related to Figure 27 with respect to the gap that exists between the absorption and scattering coefficients.

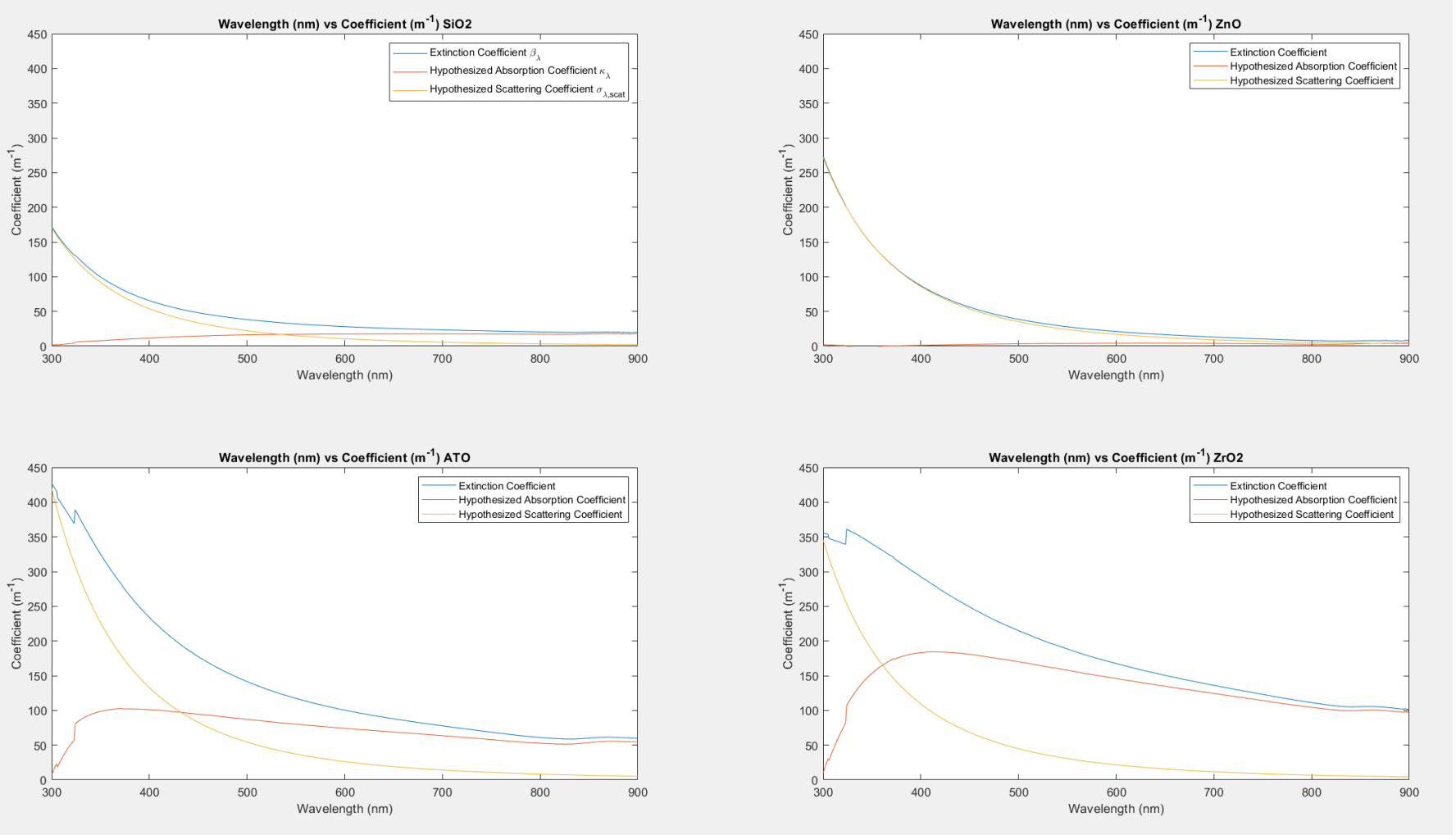

Figure 27: Spectral coefficient values for extinction, absorption and scattering based on measured transmittance data.

Chapter 7 – Thermal Characterization

7.1 Thermal Conductivity

Silica aerogels are highly porous materials with remarkable thermal insulation capabilities, making them attractive for various thermal management applications. This branch of characterization focuses on quantifying and analyzing the heat transfer behavior of aerogels, specifically effective thermal conductivity. Thermal conductivity measurements within aerogels contain three components: conduction through the silica network, conduction through the air and radiation [50]. Where radiation plays the largest role in determining the effective thermal conductivity of the aerogel. The pore sizes of the aerogel sample are small enough to neglect convection, and here we have assumed that, at least within the visible region, the air trapped within the sample's pores is smaller than the mean free path of light.

In addition to understanding the thermal properties of silica aerogels, the relationship between thermal conductivity and optical transmittance is a critical aspect of their thermal characterization. Ideally, there would be a monolithic aerogel that would have an extremely low thermal conductivity (that below air) while maintaining high visible transmittance and low infrared transmittance. Approaches to increase the thermal conductivity of aerogels include fabricating denser aerogels and or including adsorbed species within the aerogel [50]. In this work, nanoparticles were infused within silica aerogel synthesis in attempts to improve absorption within the infrared region.

Several methods have been developed to measure the thermal conductivity of silica aerogels, including the transient hot wire method, and the guarded hot plate method. These techniques involve applying a temperature gradient to the aerogel sample and measuring the resulting heat transfer.

Zhao et al. determined the thermal conductivity of a 10 mm thick silica aerogel that followed similar molar concentration ratios to range from 0.02-0.1 (W/(m·K)) [30] using a customized approach of determining the heat loss coefficient. This was based on a modified solar-thermal receiver that was attached to an electrical heater and maintained at a set temperature.

7.1.1 Modified Guarded Hot Plate

The chosen approach to measuring the thermal conductivity of the aerogel sample in this work was using an existing custom experimental apparatus developed within the Thermofluids Lab (TF-

LAB) at York University, which is based upon a modified guarded hot plate technique outlined in ASTM C177 [51]. Based on the temperature differences between the hot and cold plates, the thermal conductivity can be measured transiently using the constant electrical heat input, the thickness of the sample and the area of the heating plate. Assuming one dimensional heat transfer through the sample we can represent effective thermal conductivity as Equation 10:

$$k_{eff} = \frac{L}{A\left[\frac{\Delta T}{Q} - R_c\right]} \tag{10}$$

where k_{eff} is the effective thermal conductivity, L is the sample thickness, A is the sample cross sectional area, ΔT is the temperature difference between the top and the bottom of the sample, Q is the measured input electrical power, and R_c is the contact resistance.

7.1.1.1 Experimental Setup

The experimental setup consists of a hot plate apparatus designed to generate a controlled heat flow through the sample. The key components of the setup include a sample holder, two temperature-controlled plates (one hot and one cold), and ideally a series of guards or insulation layers surrounding the sample to minimize heat loss.

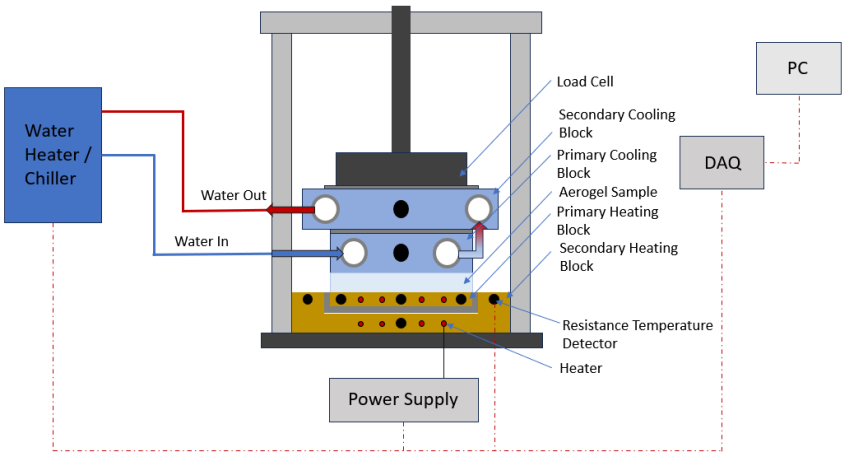

Figure 28: Modified guarded heat plate experimental apparatus overall schematic with a primary cooling block measured at 40x40 mm.

During the experiment, RTD temperature sensors are strategically positioned to measure the temperatures at different locations (as seen in Figure 28 and Figure 29), including the hot and cold plates, as well as within the sample. The heat flux and temperature differentials are recorded, and thermal conductivity is calculated using the Fourier's law of heat conduction.

Figure 29: Photograph of modified guarded heat plate experimental apparatus

Figure 30: Photograph of test section with loaded aerogel sample

The sample, in this case seen in Figure 30, a silica aerogel, is prepared and placed between the hot and cold plates, forming a thermal gradient. The hot plate is heated to a known temperature, while the cold plate is maintained at a lower temperature. The temperature difference between the plates generates a steady-state heat flow through the sample.

Overall, the guarded hot plate method provides a controlled and well-insulated setup for accurately measuring the thermal conductivity of silica aerogels but comes with the trade-off of

time-consuming measurements due to the extremely low thermal conductivity values of silica aerogels.

7.1.2 Results: Effective Thermal Conductivity

When examining experimental results that depict the effective thermal conductivity of silica aerogel samples over iterations, several observations and interpretations can be made. Firstly, while analyzing the trend of the data points, the effectiveness of the manufacturing process or any modifications made to the aerogel composition are noticeable. As the graph demonstrates a consistent decrease in thermal conductivity with each iteration, it suggests a change in the material's thermal properties as it reaches a transient state. This may be indicative of refining the synthesis technique, optimizing the pore structure, or modifying the composition of the aerogel depending on the slope of the curve as it varies per aerogel sample. Varying sample type also changes the iteration number need to reach thermal equilibrium.

Moreover, comparing the experimental results with Zhao et al.'s work similar experimentally measured silica aerogel samples helped provide confidence in the accuracy and reliability of the measured thermal conductivity values, being within the lower range of 0.02-0.1 (W/(m·K)) [30].

Furthermore, examining the scatter or dispersion of the data points on the graph helps provide insights into the reproducibility and consistency of the samples. As the data points exhibit low dispersion and are closely clustered, it suggests good reproducibility and consistency in the thermal conductivity measurements.

Overall, the analysis of experimental results through the graph of effective thermal conductivity over iterations offers valuable information about the optimization, reliability, and consistency of silica aerogel samples.

The following tests were conducted at room temperature and pressure and were performed on samples dimensioned 40 x 40 mm in size with an average thickness of 6.2 mm.

7.1.2.1 SiO_2 Aerogel Sample Thermal Conductivity Measurement

The final value of the plotted thermal conductivity graphs represents the transient effective thermal conductivity measured, with the upper and lower regions of the data being error bars. The values of the effective thermal conductivity are measured over iterations as it takes time for the measurement to reach steady state.

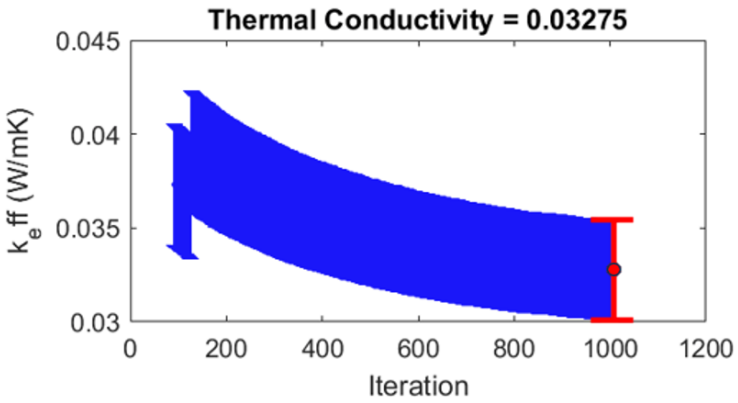

Figure 31: Effective thermal conductivity of SiO2 aerogel sample 40x40 mm with 6.3 mm thickness, reached equilibrium at 0.035 W/(m·K). Error bars include deviances noted from thermal surface contact resistance (effectively being ± 0.005 W/(m·K)).

The sudden thermal conductivity change in Figure 31 is indicative of varying the experimental parameters (cool block temperature) to prevent condensation from forming between the apparatus and the silica aerogel.

7.1.2.2 ZnO infused SiO_2 Aerogel Sample Thermal Conductivity Measurement

When conducting thermal conductivity measurements on nanoparticle infused silica aerogel samples, potential sources of error arose from the state of the samples. One factor that potentially affected the accuracy of thermal conductivity measurements (specifically for ATO and ZrO_2 infused SiO_2 silica aerogel samples as seen in Figure 32 and Figure 33) was the presence of cracks within the aerogel structure. Cracks can disrupt the heat transfer path and introduce thermal resistance, leading to potentially lower measured thermal conductivity values.

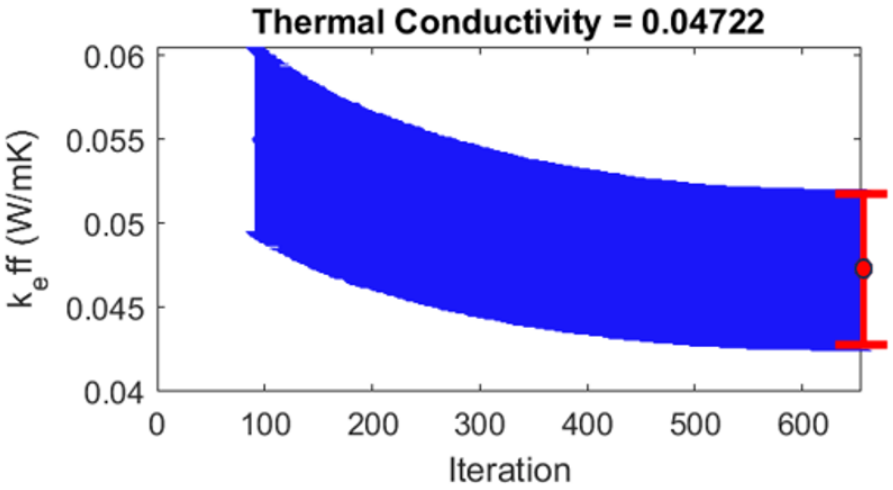

Figure 32: Effective thermal conductivity of 0.1 wt.% ZnO infused SiO2 aerogel sample 40x40 mm with 6.02 mm thickness, reached equilibrium at 0.05 W/(m·K). Error bars include deviances noted from thermal surface contact resistance (effectively being ± 0.005 W/(m·K))

7.1.2.3 ATO infused SiO_2 Aerogel Sample Thermal Conductivity Measurement

Another important consideration is the level of surface contact between the sample and the measurement device. There is potential in inaccurate thermal conductivity measurements due to incomplete contact or poor thermal coupling between the sample and the measurement apparatus as the aerogel samples had cusps near the surface (which were trimmed to the best possible extent). Variations in surface roughness, irregularities, or inadequate pressure could be reasoning behind air gaps or thermal barriers, leading to inaccurate heat transfer measurements as seen in Figure 34.

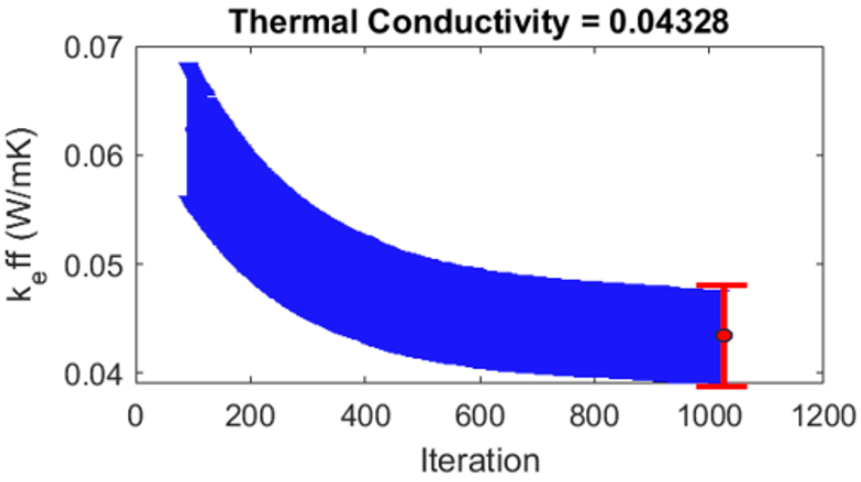

Figure 33: Effective thermal conductivity of 0.1 wt.% ATO infused SiO2 aerogel sample 40x40 mm with 6.21 mm thickness, reached equilibrium at 0.045 W(/m·K). Error bars include deviances noted from thermal surface contact resistance (effectively being ± 0.005 W/(m·K)

Furthermore, it is important to acknowledge that there can be sample-to-sample variation in the thermal conductivity of silica aerogels. Variations in the aerogel composition, density, pore structure, and synthesis conditions can all contribute to differences in thermal conductivity values. It is essential for future tests to consider this inherent variability when interpreting experimental results and to conduct enough measurements across multiple samples to account for potential variations.

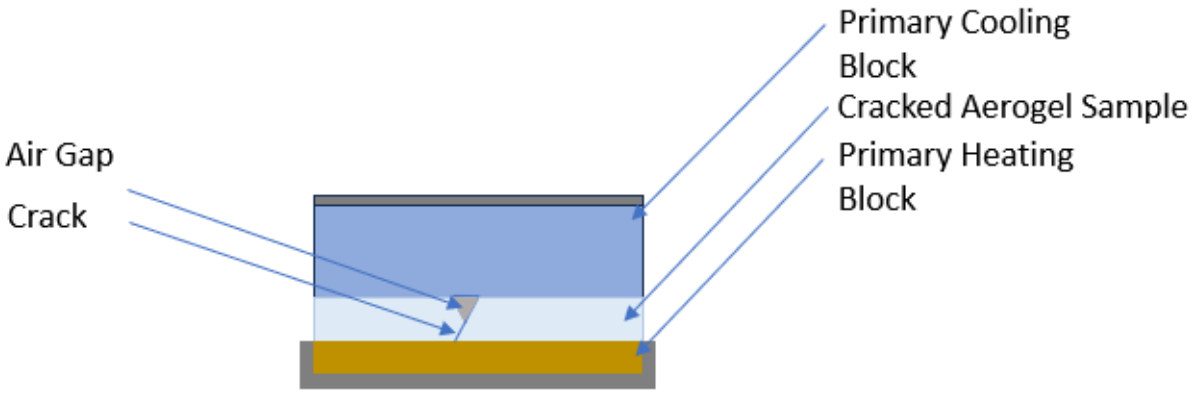

Figure 34: Cracked Aerogel simple schematic in guarded hotplate apparatus

7.1.2.4 ZrO_2 infused SiO_2 Aerogel Sample Thermal Conductivity Measurement

Verifying the accuracy of thermal conductivity measurements in silica aerogels presents a challenge, particularly when dealing with novel or unique samples. One of the reasons for this uncertainty is the absence of well-established reference materials with precisely known thermal conductivities for nanoparticle infused silica aerogels. Without suitable reference samples, it becomes challenging to validate the measurements using a direct calibration approach.

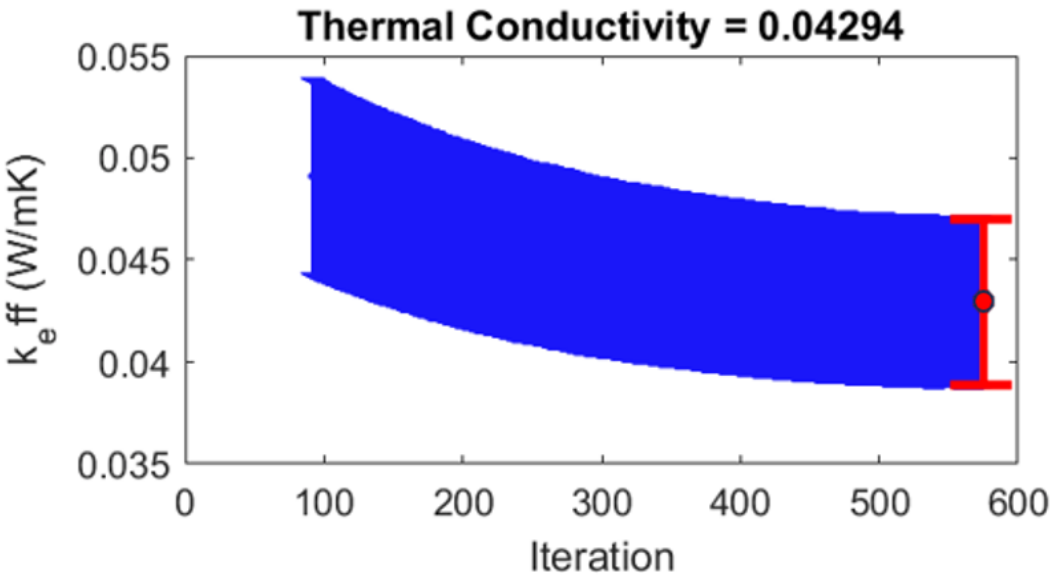

Figure 35: Effective thermal conductivity of 0.1 wt.% ZrO2 infused SiO2 aerogel sample 40x40 mm with 6.25 mm thickness, reached equilibrium at 0.045 W/(m·K). Error bars include deviances noted from thermal surface contact resistance (effectively being ± 0.005 W/(m·K)

Additionally, the wide variation in aerogel properties, such as density, pore structure, composition, and synthesis conditions, further complicates the verification process. These factors can significantly influence the thermal conductivity values, making it challenging to establish a universal benchmark for comparison. It is crucial to recognize that, due to the uniqueness and novelty of silica aerogel samples, there may still be some inherent uncertainties in verifying the thermal conductivity measurements.

7.1.2.5 Fabricated Aerogel Thermal Conductivity Summary

Table 5 provides a summary of the effective thermal conductivities of the different types of aerogels synthesized. It is important to note that only one of each sample was measured due to complexity and time required in fabrication. In comparison to the measured values, the thermal conductivity of air at room temperature and pressure is referenced as 0.02551 W/(m·K) [52], which is quite low. The SiO_2 aerogel demonstrates the lowest thermal conductivity value at 0.035 W/(m·K), indicating its excellent thermal insulation properties. The ZnO infused SiO_2 aerogel shows a slightly higher thermal conductivity of 0.05 W/(m·K), suggesting a moderate increase in heat transfer compared to pure SiO_2 aerogel. The ATO infused SiO_2 and ZrO_2 infused SiO_2 aerogels exhibit similar thermal conductivities of 0.045 W/(m·K) and 0.045 W/(m·K), respectively. These values indicate that the addition of Antimony doped Tin Oxide (ATO) or Zirconia Dioxide (ZrO_2) nanoparticles has a limited effect on the overall thermal conductivity of the aerogels in comparison to Zinc Oxide (ZnO). Overall, the results demonstrate the potential of different aerogel compositions to tailor the thermal conductivity for specific applications, with ZrO_2 infused silica aerogel exhibiting the best thermal insulating performance among the nanoparticle infused samples.

Table 5: Aerogel Thermal Conductivity Summary

Aerogel Type	Effective Thermal Conductivity (W/m·K)
SiO_2	0.035
ZnO infused SiO_2	0.050
ATO infused SiO_2	0.045
ZrO_2 infused SiO_2	0.045

Chapter 8 – Discussion & Conclusions

The discussions and conclusions drawn from the work presented here provide valuable insights into the fabrication, characterization, and performance of silica aerogels. Through a comprehensive examination of various aspects, including synthesis methods, total and direct spectral transmittance and thermal conductivity, a deeper understanding of these unique materials has been achieved. The findings highlight the influence of parameters such as nanoparticle infusion, sample thickness, and composition on the thermal and optical behavior of the aerogels. The implications of these findings extend to a wide range of applications, from thermal insulation in buildings to optical monoliths for windows. Furthermore, the uncertainties and challenges encountered during the experimental process shed light on the need for further research and development to optimize the performance of silica aerogels. By considering the discussions and conclusions presented here, future advancements in aerogel technology can be guided towards enhanced thermal insulation, improved optical properties, and expanded applications in energy-efficient and sustainable solutions.

8.1 Fabrication of Pure and Nanoparticle Infused Silica Aerogels

The fabrication of the first known nanoparticle infused SiO_2 silica aerogels was successfully achieved for introduction within wet gel synthesis as a replacement to water using water suspended nanoparticles. The results obtained align with the objectives stated in the introduction, which aimed to determine a viable method for incorporating nanoparticles into silica aerogels while maintaining monolithic integrity, optical clarity, and insulative properties. Various nanoparticles, including Zinc Oxide (ZnO), Antimony doped Tin Oxide (ATO), and Zirconia Dioxide (ZrO_2), were introduced into the Silica framework during wet-gel synthesis. Among the nanoparticle-infused silica aerogel samples, ZnO exhibited the highest monolithic integrity and optical clarity. This can be potentially attributed to the qualitatively measured solubility of ZnO in methanol during the alcohol baths in the wet-gel synthesis process (greater solubility than that of water in comparison). It is hypothesized that some nanoparticles may have dissolved or been removed from the silica framework during the alcohol exchanges. On the other hand, ZrO_2 showed the least optical clarity, displaying a cloudy or hazed appearance. All nanoparticle-infused silica aerogel samples retained cusp-like formations on the surface exposed to liquid CO_2 during supercritical drying and were observed to be more fragile compared to pure silica aerogels,

evidenced by a history of cracking during storage under non-linear and rapid pressure changes (when stored in near-vacuum from room pressure). Furthermore, the nanoparticle-infused samples required trimming with a sharp blade to achieve a flat surface for thermal conductivity measurements using the guarded hot plate method.

Throughout the research, several limitations and challenges were encountered, which are essential to address. The constructed manuclave (Figure 7) had limited space for aerogel drying (approximately 2 inches), which restricted the size of the aerogel samples and maintaining a constant pressure bleed rate in the manuclave proved challenging. The homogeneity and solubility of the aerogels were potentially affected by their reactivity with different alcohols and liquid CO_2 during the drying process. Notably, the aerogel samples formed cusps during drying due to the pressure exerted during the drying procedure and their hydrophilic nature. One of the notable challenges involved the gelation of aerogel samples with Antimony doped Tin Oxide (ATO) nanoparticles, which was difficult to achieve without cracking. Moreover, the materials used as assistance for aerogel synthesis (gaskets, molds) were sensitive to deformation when placed in the supercritical region of CO_2, limiting their application. The aerogel samples during supercritical drying also had different surface finishes based on the surface interacting with liquid CO_2 and the surface facing the mold. The catalyst solution and nanoparticle suspensions had a limited shelf life, leading to slowed reactions, fallout of suspension, or agglomeration. The fast gelation time posed difficulties in addressing issues that could have arisen during solution pouring, such as bubbles from pipetting or variation in recipe procedures. Adhesion of the sample to the pipette tips also resulted in mild inaccuracies in the recipe volume, despite attempts to condition the tips with the solution beforehand. There was a potential risk of cross-contamination between samples during alcohol baths even though the baths contained the same material. During the baths, there were often small shards of aerogel samples found when exchanging for fresh alcohol, insinuating shrinkage and or a reaction continuously occurring. Homogeneity of the sample was crucial, as nanoparticles had the tendency to sink or collect in specific areas during gelation. Achieving stability in the nanoparticle solution was essential for the structural integrity and optical clarity of the resulting aerogel samples. Balancing the precursor, catalyst, and solvent was critical, particularly in terms of nanoparticle dispersion weight percentage.

8.2 Optical Transmittance

In terms of transmittance, the measurements provide information about the aerogels' ability to transmit light across different wavelengths. The variations in transmittance values can be attributed to factors such as scattering, absorption, and the presence of nanoparticles. These findings have implications for applications where optical properties, such as visible light transmittance, are crucial. It allows for the selection of aerogel compositions that balance both thermal insulation and desirable optical characteristics.

8.2.1 Spectrophotometry

The spectrophotometric measurements provided valuable insights into the optical properties of the nanoparticle-infused silica aerogel samples. The direct transmittance values were measured, and the solar weighted mean transmittance was determined. Among the nanoparticle-infused samples, the ZnO infused SiO_2 exhibited the highest direct transmittance in the visible range, followed by ZrO_2 and ATO infused Silica aerogels. These findings align with the objective of comparing the transmittance of the nanoparticle-infused samples to the pure SiO_2 samples. It was observed that ZnO and ZrO_2 infused SiO_2 aerogels behaved similarly to pure silica aerogels in the visible range, while ATO infused sample showed distinct patterns with lower transmittance and higher absorbance beyond 1000 nm. The different slopes of the transmittance curves within the visible region corresponded to the scattering and absorption characteristics of each aerogel. Notably, ZnO exhibited the lowest scattering behavior, followed by ZrO_2 and ATO. Interestingly the ZnO infused sample scattered less in the visible region than the pure silica aerogel which is hypothesized to be due to excess ZnO nanoparticles being potentially evacuated during alcohol exchange during wet gel synthesis (removed from the aerogel). In the infrared region, small absorption peaks were observed in the early 1000 nm range, mentioned in literature as being attributed to adsorbed nanoparticle solution or water on the surface of the silica particles [5]. Additionally, larger peaks were observed beyond 3000 nm, with pure SiO_2 showing the highest transmittance, followed by ZrO_2, ZnO, and ATO infused samples. The unique behavior of each nanoparticle-infused aerogel can be further explored, including the potential impact of the confidential surfactant used during nanoparticle stock formation for ATO. The results indicate the complex interplay between nanoparticle composition and the optical properties of the aerogels, providing valuable insights for their potential uses.

During spectrophotometric measurements, one of the challenges encountered was maintaining the same area of measurement between the spectrophotometers for the same sample between differing machines. Since the nanoparticles infused inside the aerogel samples might not have been uniformly distributed across the volume, it was difficult to ensure that the exact same area was being measured in each sample. This variability in nanoparticle spread within the aerogel could potentially introduce inconsistencies in the measured transmittance values. It is important to consider this limitation when interpreting the results across machinery and discussing the optical properties of the nanoparticle-infused silica aerogels. Further research and development can explore methods to improve the uniformity of nanoparticle distribution within the aerogel samples, thereby enhancing the reliability and accuracy of the optical characterization.

8.2.2 Simple Numerical Model

The optical behavior of silica aerogels was further investigated in this study using a simple numerical model, revealing interesting characteristics of the samples in different wavelength regions. The results indicate that the aerogels exhibit optically thin behavior within the visible region, while transitioning to an optically thick regime in the infrared (IR) region. The thickness of the aerogel sample also plays a role in its optical behavior. In the optically thin limit, where the sample thickness is much smaller than the incident light's wavelength, the aerogel appears transparent. This is particularly noticeable in the visual range. On the other hand, reaching an optically thick limit, especially in the infrared region, is desirable for enhancing the aerogel's thermal insulative properties. The transition between the optically thin and optically thick limits can vary based on the composition, density, and thickness of the aerogel sample. This finding aligns with the expected behavior of aerogels, as Rayleigh scattering dominates at shorter wavelengths. The spectral transmittance data is correlated with the modeled Rayleigh scattering coefficient, indicating a stronger scattering behavior in the UV and visible range. The total transmittance, incorporating both scattering and absorption properties, provides valuable insights into the overall light transmission through the aerogels.

It is important to note that the simple numerical model used in this study, based on Rayleigh theory, has its limitations. The assumptions made in the model, such as uniform particle sizes and purely scattering behavior, may not hold true for all cases, especially when nanoparticle-infused aerogels are involved. Furthermore, the absorption coefficient becomes a dominant factor

beyond the visible region, while scattering remains the dominant behavior in the UV and visible range.

8.3 Thermal Conductivity

The findings of thermal conductivity and transmittance measurements for the fabricated aerogel samples have important implications. The observed thermal conductivities provide insights into the effectiveness of the aerogels as thermal insulators. Lower thermal conductivity values, such as those exhibited by the pure SiO_2 aerogel, indicate higher insulation capabilities, making them suitable for applications where heat transfer reduction is desired. On the other hand, the variations in thermal conductivity among the infused aerogels (ZnO infused SiO_2, ATO infused SiO_2, and ZrO_2 infused SiO_2) suggest that the addition of nanoparticles may slightly affect the thermal properties of the aerogels.

One significant challenge was achieving full surface contact between the aerogel samples and the measurement apparatus. The formation of cusps on the surface of the aerogel samples created uneven contact, making it difficult to establish consistent thermal conductivity measurements. Additionally, the use of thermal paste to enhance contact was not feasible in this study. The necessity for insulation and guards around the samples further complicated the measurement process. Furthermore, the density and porosity of the aerogel samples were hypothesized to affect their thermal conductivity, highlighting the need to investigate the measured porosity of the nanoparticle dispersions. Comparisons were made between the thermal conductivity of the fabricated SiO_2 aerogel samples and the values reported by Zhao et al [30], which allowed for a baseline measurement and some level of validity to the nanoparticle infused samples. The influence of different nanoparticles, particularly ZrO_2, on the thermal conductivity of the aerogels was also examined, where the ZrO_2 infused SiO_2 sample had the lowest thermal conductivity measurement. This may have been attributed to the state of the sample, containing air gaps and cracks. Going past the experimental flaws, if the measured thermal conductivity matches the sample, it provides insight to uses of different nanoparticles that work well for their characteristic properties to be infused within silica aerogels. Interestingly, the ZnO infused silica aerogel had the highest thermal conductivity measurement, considering it performed optimally within the optical region, this trade-off is expected. The ATO infused silica aerogel sample shows a balance between optical and thermal properties, while maintaining in the middle of the

nanoparticle samples for thermal conductivity and having the strongest absorption properties within the optical region.

It is important to note that the optical thickness of the aerogels and their thermal conductivity may have varying effects on the heating behavior of the material. Further investigations are required to fully understand and elucidate these complex relationships.

8.4 Summary Statement

In this study, nanoparticle infused SiO_2 samples were successfully synthesized with the aim of achieving optimized optothermal characteristics, with the first pure silica and nanoparticle infused silica aerogel samples being fabricated on York University grounds. The experimental results indicated that among the fabricated samples, ZnO infused Silica aerogels exhibited the most desirable behavior in terms of both thermal and optical properties. The direct and hemispherical transmittance of each sample was measured to assess their optical performance, while the effective thermal conductivity was determined to evaluate their thermal characteristics. Overall, the findings suggest that ZnO-infused SiO_2 samples hold promise for applications requiring favorable thermal and optical properties due to their high visible transmittance, low infrared transmittance and low thermal conductivity values in relation to the compared nanoparticle infused samples, with visible transmittance closely comparable to the synthesized pure silica aerogel.

8.4.1 Future Work

To further advance the understanding and optimize the properties of nanoparticle-infused silica aerogels, several future considerations can be explored. One potential avenue is to investigate the effects of varying the types of nanoparticle mixtures infused in the silica aerogel. Additionally, a study focused on sample shrinkage is warranted to examine how the presence of nanoparticles influences the shrinkage behavior and shape of the aerogel during drying and storage based on more realistic environments such as that in a double paned window. Temperature annealing can also be explored as a method to induce property changes in the aerogels, potentially altering their thermal conductivity or optical behavior. Considerations should also be given to wrap the aerogels with aluminum tape during spectrophotometric measurements to improve the accuracy of the obtained optical data. Further research into the usage of surfactants in dispersion is needed to investigate their impact on the optical and thermal properties of the aerogels. Moreover,

morphological characterization can be included to measure the pore size distribution and average pore size can through techniques such as porosimetry, providing valuable information about the structural properties of the aerogels.

An optimized procedure for nanoparticle infusion during synthesis should be developed, aiming for better adhesion, and reducing the number of steps involved. Considerations for molds, including the use of gaskets and alternative mold release methods, need to be explored to address issues related to cracking, shrinking, and the appearance of residual layers during alcohol baths. The noteworthy influence of weight percentage on agglomeration and the distinct visual appearance differences, such as the blue haze observed in ATO-infused SiO_2 samples (separate from Rayleigh scattering) and the white haze in ZrO_2-infused samples, should be further investigated and understood.

To ensure accurate measurements, the thermal conductivity measurement setup should be carefully designed to minimize heat losses to the surroundings. This can be achieved by incorporating guard layers around the sample, which function as thermal barriers to reduce heat transfer by conduction and convection. The guards help create an isothermal environment around the sample, allowing for a more precise determination of thermal conductivity. Originally, Kapton tape is used to surround the sample as insulation, unfortunately tape and adhesives have a difficulty adhering to aerogels due to their porous structures.

Lastly, Monte Carlo ray tracing and scattering simulations can be employed to simulate and analyze the scattering behavior of the aerogels, enhancing the understanding of their optical characteristics. These future considerations will contribute to the ongoing exploration of nanoparticle-infused silica aerogels and pave the way for further optimization and advancements in their properties and applications.

References

[1] L. Fernandez, “Global primary energy consumption 2021 | Statista,” 2023. [Online]. Available: https://www.statista.com/statistics/265598/consumption-of-primary-energy-worldwide/. [Accessed: 08-Jul-2023].

[2] IEA (2023), Tracking Clean Energy Progress 2023, IEA, Paris. [Online] Available: https://www.iea.org/reports/tracking-clean-energy-progress-2023, License: CC BY 4.0. [Accessed: 08-Jul-2023]

[3] “Heating – Analysis - IEA,” *IEA Energy-System / Buildings / Heating*, 2023. [Online]. Available: https://www.iea.org/reports/heating. [Accessed: 08-Jul-2023].

[4] R. B. Wendell E. Rhine, Ying Tang, Wenting Dong, Roxana Trifu, “Highly Insulating Windows with a U-value less than 0 . 6 W / m 2 K,” *Contract*, 2008.

[5] L. Zhao *et al.*, “Harnessing Heat beyond 200 °c from Unconcentrated Sunlight with Nonevacuated Transparent Aerogels,” *ACS Nano*, 2019, doi: 10.1021/ACSNANO.9B02976/SUPPL_FILE/NN9B02976_SI_001.PDF.

[6] C. Buratti, E. Belloni, F. Merli, and M. Zinzi, “Aerogel glazing systems for building applications: A review,” *Energy Build.*, vol. 231, p. 110587, Jan. 2021, doi: 10.1016/J.ENBUILD.2020.110587.

[7] H. Gunes, Y. Özbakir, S. B. Barim, H. Yousefzadeh, S. E. Bozbag, and C. Erkey, “A Remarkable Class of Nanocomposites: Aerogel Supported Bimetallic Nanoparticles,” *Front. Mater.*, vol. 7, p. 507369, Feb. 2020, doi: 10.3389/FMATS.2020.00018/BIBTEX.

[8] F. Matter, A. L. Luna, and M. Niederberger, “From colloidal dispersions to aerogels: How to master nanoparticle gelation,” *Nano Today*, vol. 30, p. 100827, 2020, doi: 10.1016/j.nantod.2019.100827.

[9] I.-K. Jung, J. L. Gurav, T.-J. Ha, S. G. Choi, S. Baek, and H.-H. Park, “The properties of silica aerogels hybridized with SiO 2 nanoparticles by ambient pressure drying,” *Ceram. Int.*, vol. 38, pp. S105–S108, 2011, doi: 10.1016/j.ceramint.2011.04.060.

[10] M. Li *et al.*, “Ultralight and Flexible Monolithic Polymer Aerogel with Extraordinary Thermal Insulation by A Facile Ambient Process,” *Adv. Mater. Interfaces*, vol. 6, no. 13, p. 1900314, 2019, doi: https://doi.org/10.1002/admi.201900314.

[11] “Aerogel.org » What is Aerogel?” [Online]. Available: http://www.aerogel.org/?p=3. [Accessed: 22-Aug-2023].

[12] M. A. Worsley and T. F. Baumann, “Carbon Aerogels,” *Handb. Sol-Gel Sci. Technol.*, pp. 1–36, 2016, doi: 10.1007/978-3-319-19454-7_90-1.

[13] Y. Wu, X. Wang, and J. Shen, “Metal oxide aerogels for high-temperature applications,” *J. Sol-Gel Sci. Technol.*, vol. 106, no. 2, pp. 360–380, May 2022, doi: 10.1007/S10971-021-05720-W/FIGURES/1.

[14] L. Zuo, Y. Zhang, L. Zhang, Y. E. Miao, W. Fan, and T. Liu, “Polymer/Carbon-Based Hybrid Aerogels: Preparation, Properties and Applications,” *Materials (Basel).*, vol. 8, no. 10, p. 6806, 2015, doi: 10.3390/MA8105343.

[15] A. M. Anderson and M. K. Carroll, “Hydrophobic Silica Aerogels: Review of Synthesis,

Properties and Applications," *Aerogels Handb.*, pp. 47–77, 2011, doi: 10.1007/978-1-4419-7589-8_3.

[16] M. Freire-Gormaly, J. S. Ellis, H. L. MacLean, and A. Bazylak, "Pore Structure Characterization of Indiana Limestone and Pink Dolomite from Pore Network Reconstructions," Oil Gas Sci. Technol., vol. 71, no. 3, p. 33, 2015.

[17] M. Freire-Gormaly, J. S. Ellis, A. Bazylak, and H. L. MacLean, "Comparing thresholding techniques for quantifying the dual porosity of Indiana Limestone and Pink Dolomite," Microporous Mesoporous Mater., vol. 207, pp. 84–89, May 2015.

[18] M. Freire-Gormaly, "The Pore Structure of Indiana Limestone and Pink Dolomite for the Modeling of Carbon Dioxide in Geologic Carbonate Rock Formations," University of Toronto, 2013.

[19] H. S. H. Nguyen *et al.*, "Insights into sustainable aerogels from lignocellulosic materials," 2022, doi: 10.1039/d2ta04994e.

[20] M. Freire-Gormaly and A. M. Bilton, "Design of photovoltaic powered reverse osmosis desalination systems considering membrane fouling caused by intermittent operation," *Renew. Energy*, vol. 135, pp. 108–121, 2019, doi: 10.1016/j.renene.2018.11.065.

[21] L. Horrigan and M. Freire-gormaly, "Modelling the effects of ultrasonic sonification on reverse osmosis feed channel temperature," *Desalination*, vol. 521, no. August 2021, p. 115332, 2022, doi: 10.1016/j.desal.2021.115332.

[22] M. Freire-Gormaly and A. M. Bilton, "Experimental quantification of the effect of intermittent operation on membrane performance of solar powered reverse osmosis desalination systems," *Desalination*, 2017, doi: http://www.sciencedirect.com/science/article/pii/S0011916417311104.

[23] M. Freire-Gormaly and A. M. Bilton, "Impact of intermittent operation on reverse osmosis membrane fouling for brackish groundwater desalination systems," *J. Memb. Sci.*, vol. 583, pp. 220–230, 2019, doi: 10.1016/j.memsci.2019.04.010.

[24] M. Freire-Gormaly and A. M. Bilton, "An experimental system for characterization of membrane fouling of solar photovoltaic reverse osmosis systems under intermittent operation," *Desalin. Water Treat.*, vol. 73, pp. 54–63, 2017, doi: 10.5004/dwt.2017.20391.

[25] M. Freire-Gormaly and A. M. Bilton, "Degradation of Photovoltaic Reverse Osmosis Systems under Intermittent Operation," in *EDS Desalination for the Environment*, 2016, pp. 1–7.

[26] M. Freire-Gormaly, "Experimental Characterization of Membrane Fouling under Intermittent Operation and Its Application to the Optimization of Solar Photovoltaic Powered Reverse Osmosis Drinking Water Treatment Systems," University of Toronto, 2018.

[27] K. Al-Marzoki, "Effect of Tetraethoxysilane and Tetramethoxysilane (TEOS/TMOS) on Melting Gel Behavior," *PhD Thesis*, 2018.

[28] M. Grogan, "Silica Aerogel (TMOS, Base-Catalyzed)," *The Critical Point (How to Make Silica Aerogels: Part 1)*. [Online]. Available: http://www.aerogel.org/?p=1406.

[29] M. David and W. Grogan, "Aerogel and Fibre Optics," 2010.

[30] L. D. M. I. of T. Zhao, “Radiative transport in transparent aerogels for solar thermal energy applications,” 2019.

[31] “Making a remarkable material even better | MIT News | Massachusetts Institute of Technology.” [Online]. Available: https://news.mit.edu/2020/making-remarkable-material-even-better-aerogel-0225. [Accessed: 12-Jun-2023].

[32] E. Cohen and L. Glicksman, “Thermal Properties of Silica Aerogel Formula,” *J. Heat Transfer*, vol. 137, p. 81601, 2015, doi: 10.1115/1.4028901.

[33] C. Mandal, Suraj Donthula, R. Soni, M. Bertino, Chariklia Sotiriou-Leventis, and Nicholas Leventis, “Light scattering and haze in TMOS-co-APTES silica aerogels,” *J. Sol-Gel Sci. Technol.*, vol. 90, pp. 127–139, 2019, doi: 10.1007/s10971-018-4801-0.

[34] “Parts and Schematics,” *Open Source Nanotech*. [Online]. Available: http://www.aerogel.org/?p=667.

[35] A. Pisal and A Venkateswara Rao, “Comparative studies on the physical properties of TEOS, TMOS and Na 2 SiO 3 based silica aerogels by ambient pressure drying method,” doi: 10.1007/s10934-016-0215-y.

[36] A. S. Dorcheh and M. H. Abbasi, “Silica aerogel; synthesis, properties and characterization,” 2007, doi: 10.1016/j.jmatprotec.2007.10.060.

[37] A. Venkateswara Rao, G. M. Pajonk, D. Haranath, and P. B. Wagh, “Effect of Sol-Gel Processing Parameters on Optical Properties of TMOS Silica Aerogels,” *J. Mater. Synth. Process.*, vol. 6, no. 1, pp. 37–48, 1998, doi: 10.1023/A:1022607125715.

[38] B. Tan and S. E. Rankin, “Study of the Effects of Progressive Changes in Alkoxysilane Structure on Sol-Gel Reactivity,” 2006, doi: 10.1021/jp060376k.

[39] “Aerogel.org » Production of Silica Gels: Alkoxide Method.” [Online]. Available: http://www.aerogel.org/?p=90. [Accessed: 17-Aug-2023].

[40] E. Strobach, B. Bhatia, S. Yang, L. Zhao, and E. N. Wang, “High temperature stability of transparent silica aerogels for solar thermal applications,” *APL Mater.*, vol. 7, no. 8, 2019, doi: 10.1063/1.5109433.

[41] “File:Carbon dioxide isotherms-en.svg - Wikimedia Commons.” [Online]. Available: https://commons.wikimedia.org/wiki/File:Carbon_dioxide_isotherms-en.svg. [Accessed: 16-Jun-2023].

[42] T. G. Schaefer, “Effects of Varying Ethanol and Water Concentrations as a Gold Nanoparticle Gel Solvent.”

[43] Z. Song *et al.*, “Characterization of optical properties of ZnO nanoparticles for quantitative imaging of transdermal transport,” *Biomed. Opt. Express*, vol. 2, no. 12, p. 3321, Dec. 2011, doi: 10.1364/BOE.2.003321.

[44] T. D. K. et Al., “Effects of incorporating ZnO on characteristic, performance, and antifouling potential of PSf membrane for PRW treatment,” *IOP Conf. Ser. Mater. Science Eng.*, 2021, doi: 10.1088/1757-899X/1053/1/012134.

[45] E. G. Goh, X. Xu, and P. G. Mccormick, “Effect of particle size on the UV absorbance of zinc oxide nanoparticles,” 2014, doi: 10.1016/j.scriptamat.2014.01.033.

[46] G. Jain and R. Kumar, “Electrical and optical properties of tin oxide and antimony doped

tin oxide films," doi: 10.1016/j.optmat.2003.12.006.

[47] S. Naya, Y. Shite, and H. Tada, "Photothermal effect of antimony-doped tin oxide nanocrystals on the photocatalysis," *Catal. Commun.*, vol. 142, p. 106044, Jul. 2020, doi: 10.1016/J.CATCOM.2020.106044.

[48] L. Zhao, S. Yang, B. Bhatia, E. Strobach, and E. N. Wang, "Modeling silica aerogel optical performance by determining its radiative properties," *AIP Adv.*, vol. 6, no. 2, 2016, doi: 10.1063/1.4943215.

[49] V. V Tuchin, "Polarized light interaction with tissues," *J. Biomed. Opt*, vol. 21, no. 7, p. 71114, 2016, doi: 10.1117/1.JBO.21.7.071114.

[50] L. A. Weinstein, G. Chen, C. R. Soderberg, R. Aeyaratne, and Q. Berg, "Improving solar thermal receiver performance via spectral and directional selectivity," 2017.

[51] A. Elkholy, M. Rouby, and R. Kempers, "Characterization of the anisotropic thermal conductivity of additively manufactured components by fused filament fabrication," *Prog. Addit. Manuf.*, vol. 4, no. 4, pp. 497–515, 2019, doi: 10.1007/s40964-019-00098-2.

[52] Y. Cengel and A. Ghajar, *Heat and Mass Transfer*, 5th ed. McGraw-Hill, 2015.

Appendices

APPENDIX A: Detailed Procedure for Supercritical Drying of Silica Aerogels with CO_2

8.4.1.1Procedure Remarks

Safety: When performing this procedure, it is essential to prioritize safety. Follow all safety guidelines and wear appropriate personal protective equipment (PPE) such as gloves, goggles & face shield, and lab coats. Ensure proper ventilation in the working area and be cautious when handling high-pressure equipment.

Equipment Calibration: Before starting the drying process, ensure that all equipment, including the chiller/heater, torque wrench, pressure release valve, CO_2 tank, and manuclave, are properly calibrated, have no leaks, are filled, and in good working condition. Regularly check and maintain the equipment to ensure accurate and reliable results.

Pressure Monitoring: Throughout the procedure, carefully monitor the pressure within the manuclave and adjust as necessary to prevent overpressure (follow Figure 36). Sudden pressure changes or excessive pressure can lead to equipment failure, sample damage or the rupture disk / emergency release being activated. It is important to note that the occurrence of boiling, indicated by rising bubbles, can indicate pressure leaks and should be monitored to maintain the integrity of the drying process.

Liquid CO_2 Level: Pay close attention to the liquid CO_2 level during the entire process. It should never fall below the sample. If needed, observe the level through the window and adjust accordingly to maintain a consistent liquid CO_2 bath.

Sample Security: Take extra precautions to securely place the sample inside the manuclave, ensuring it is well-protected and will not be affected by liquid CO_2 raining or turbulent flow. Properly wrap the pipe-plug-window with nickel Teflon to prevent any leaks or loss of CO_2.

Repeated Cycles: The draining and recharging cycles are essential to remove residual ethanol and ensure optimal supercritical drying. Repeat the cycles at least three times to ensure thorough removal of the solvent.

Proper Shutdown: When depressurizing and shutting down the supercritical dryer, follow the steps meticulously to ensure a controlled release of pressure and prevent any accidents or sample damage.

By following this procedure diligently, you can achieve successful supercritical drying of silica aerogel samples, leading to the production of high-quality aerogels with remarkable properties suitable for various applications.

1. **Prepare the Supercritical Dryer:**

a. Turn on the chiller/heater and set it to 7 degrees Celsius, allowing the manuclave to reach a temperature of 10 degrees.

b. Ensure the sample is securely placed inside the manuclave, taking precautions against exposure to raining liquid CO_2.

c. Apply 4-5 wraps of nickel-Teflon (nickel-PTFE) to the pipe-plug-window.

d. Use a torque wrench to tighten the pipe-plug-window to 86 lb-ft.

e. Close all other valves and fully open the CO_2 tank valve.

f. Slowly open the manuclave CO_2 inlet valve while maintaining a slow bleed rate, allowing pressure to reach between 650 and 850 psi over a period of 2 minutes (at 650 psi and 7 degrees Celsius CO_2 starts forming into a liquid).

g. Once a stable pressure is reached, fully open the manuclave CO_2 inlet valve.

h. Place a 500 mL beaker under the main drain located at the bottom of the manuclave.

i. Slowly bleed the main drain while collecting the solvent (ethanol) for about 10 minutes, ensuring that the collected liquid represents 50-70% of the solvent. If the valve does not bleed, close and re-open it to clear any ice blockages. Also, ensure that the liquid CO_2 level never falls below the sample.

j. Close the main drain valve.

k. Open the pressure release valve slowly until a hissing sound is heard.

l. Allow the liquid CO_2 to refill the manuclave for 10-15 minutes. Again, ensure that the liquid CO_2 level never falls below the sample.

m. Close the pressure release valve and allow the sample to rest in the liquid CO_2 for 24 hours.

2. **Drain and Recharge the Supercritical Dryer:**

a. Slowly open the main drain valve to drain the CO_2 and residual ethanol for 10-20 minutes, ensuring the liquid CO_2 level never falls below the sample.

b. Close the main drain valve.

c. Open the pressure release valve until a hissing sound is heard.

d. Allow the liquid CO_2 to refill the manuclave for 10-15 minutes, once again ensuring the liquid CO_2 level never falls below the sample.

e. Close the pressure release valve.

f. Allow the sample to sit in the liquid CO_2 bath for another 24 hours.

g. Repeat the drain and recharge procedure at least three times.

3. **Supercritical Drying:**

a. Close all valves, including the CO_2 tank valve.

b. Wipe all surfaces dry.

c. Set the chiller/heater to 80 degrees Celsius.

d. Wait for the manuclave to approach 40 degrees Celsius and 1200 psi. As the temperature rises, monitor the pressure, and release it, as necessary.

e. When the manuclave temperature reaches between 33 and 35 degrees Celsius, set the chiller/heater to 45 degrees (this value may vary depending on the insulation covering the manuclave / heat loss, the idea being to maintain the temperature and pressure above the supercritical point of CO_2).

f. The pressure should be at least 1071 psi by 31.3 degrees Celsius (refer to Figure 36).

g. The heating process should occur over a 30–45-minute time.

h. Once the manuclave reaches a stable 40 degrees Celsius and 1200 psi, leave the sample in this state for 30-60 minutes.

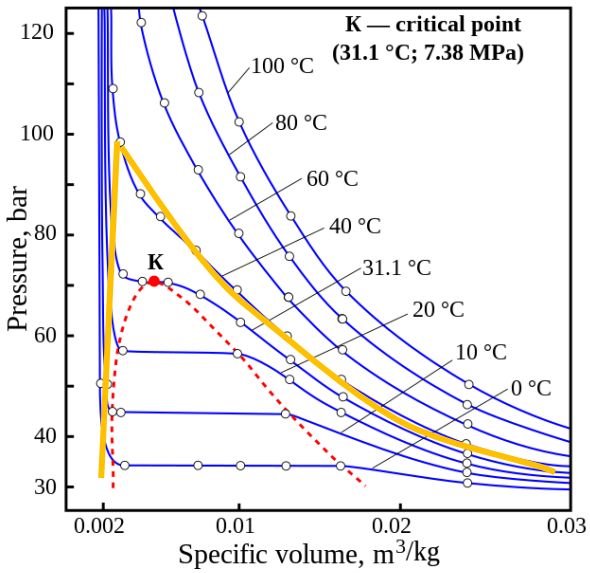

Figure 36: CO_2 isotherm, showing the pressure and specific volume followed for supercritical drying. The area above and to the right of the red line and dot represents the supercritical region. The orange line roughly being the process followed during synthesis at York University [41]

4. **Post-Supercritical Procedure (Draining & Depressurizing):**

a. Slowly open the main drain valve to release pressure with a slow bleed rate (10-20 psi per minute ideally), ensuring that the pressure reaches 500 psi within 30-60 minutes.

b. When 500 psi is reached, gradually release more pressure until it reaches ambient pressure within 10-20 minutes.

c. Carefully and fully open the main drain valve.

d. Carefully and fully open the pressure release valve.

e. Using the breaker bar, open the pipe-plug-window.

f. Remove the sample from the manuclave.

g. Slowly open the manuclave CO_2 inlet valve while ensuring the CO_2 tank valve is fully closed.

h. Admire your successfully super critically dried silica aerogel sample!